CO_2 Capture from Dilute Sources via Lime-Based Sorbents

By

Mohammad Samari

Thesis submitted to the Faculty of Graduate and Postdoctoral Studies

In partial fulfillment of the requirements for the

M.A.Sc degree in Chemical Engineering

Department of Chemical and Biological Engineering

University of Ottawa

March 2014

Statement of Contribution of Collaborators

I am the sole author of all the chapters of this thesis. My supervisors, Dr. Arturo Macchi of the Department of Chemical and Biological Engineering, University of Ottawa, and Dr. Edward John Anthony of CanmetENERGY, Natural Resources Canada, supervised my work during the M.A.Sc. program and provided editorial corrections.

Signature: _____ Date: _____

Abstract

Direct capture of CO_2 from ambient air is a developing technology, which is capable of removing CO_2 directly from the atmosphere. Moreover, this technology is independent from sources of CO_2 emissions. Hence, it can be set up at locations where pure stream of CO_2 is needed such as in enhanced oil recovery.

In this research, the performance of pelletized and natural limestone for CO_2 capture from air in a fixed bed is studied. To compare the performance of sorbents for air capture, the effects of particle type (natural limestone and pelletized limestone), particle size (250-425 μm and 425-600 μm), gas flowrate (0.5 L/min and 1 L/min), and relative humidity, on the breakthrough time, breakthrough shape, and the global reaction rate are examined. Moreover, carbonation decay of sorbents over series of capture and regeneration cycles is studied.

If the inlet stream (air) is humidified at 50% relative humidity, but the lime sorbents are not pre-hydrated, an axially non-uniform carbonated bed results. This phenomenon is due to the partial carbonation of sorbents at the first layers of the bed. While there is a competition between CO_2 and water to react with CaO, partial carbonation reaction on the surface of the sorbents not only prevents further hydration, but also decreases the reaction rate at the surface. However, in comparison with a dry system where relative humidity was negligible and sorbents were not pre-hydrated, the observed carbonation conversion was higher. The best results were seen from experiments with pre-hydrated sorbents and humidified inlet stream.

The smaller sorbent particles had a better performance (sharper breakthrough curve and longer breakthrough time) due to their greater surface area. A gas-solid reaction model was fitted to the breakthrough curves. Since at the beginning of carbonation there is no resistance of the product layer, it can be assumed that the process is reaction controlled. While after formation of the product layer ($CaCO_3$), it becomes diffusion controlled. Results from fitted data also confirmed these conclusions. Moreover, each of sorbent went through 9 cycles and after each cycle the carbonation conversion of the sorbents was measured by TGA and the surface area by BET.

Sommaire

La capture directe de CO_2 de l'air ambiant est une technologie en développement qui est capable d'éliminer le CO_2 à partir de l'atmosphère directement. De plus, cette technologie est indépendante de sources qui émettent le CO_2. Ainsi, elle peut être installée aux endroits où un flux pur du CO_2 est nécessaire; un exemple est dans la récupération améliorée du pétrole.

Dans cette recherche, la performance de la chaux granulé et la chaux naturel pour la capture du CO_2 de l'air a été étudiée dans un lit fixe. Pour comparer la performance des sorbants pour la capture de l'air, les effets du type des particules (la chaux naturelle et la chaux granulée), la taille des particules (250-425 µm et 425-600 µm), le débit du gaz (0.5 L/min and 1 L/min), et l'humidité relative, sur le temps de «breakthrough», la forme de breakthrough, et le taux de réaction globale ont été examinées. Par ailleurs, la carbonation décroissante du sorbant au cours des cycles de capture et de régénération ont été étudiée.

Si le courant d'entrée (l'air) est humidifié à l'humidité relative de 50%, mais les sorbants de chaux ne sont pas hydratés en avance, cela crée un axialement non-uniforme lit carbonaté. Ce phénomène est le résultat de la carbonatation partielle de sorbants dans les premières couches du lit. Alors qu'il y a une compétition entre le CO_2 et l'eau pour réagir avec CaO, la réaction de la carbonatation partielle sur la surface des sorbants non seulement empêche plus d'hydratation, mais également diminue la vitesse de la réaction sur la surface. Toutefois, la comparaison avec un système sec, où l'humidité relative était

négligeable et sorbants n'ont pas été hydratés à l'avance, la conversion de la carbonatation observée est plus élevée. Les meilleurs résultats ont été observés dans les expériences avec les sorbants qui ont été hydratés à l'avance et humidifié dans lecourant d'entrée.

Les petites particules de sorbant avaient une meilleure performance (les courbes de la breakthrough plus nette et les temps de la breakthrough plus long) en raison de leur plus grande surface. Un modèle de réaction gaz-solide a été ajusté aux courbes de la breakthrough. Étant donné qu' au début de la carbonatation il n'y a pas de résistance de la couche de produit, on peut supposer que le procédé est contrôlé par la réaction. Bien qu'après la formation de la couche de produit ($CaCO_3$), le procédé devient contrôlé par la diffusion. Résultats de données ajustées ont également confirmé ces conclusions. De plus, chacun des sorbants a traversé 9 cycles et après chaque cycle la conversion de la carbonatation des sorbants a été mesurée par ATG (L'analyse thermogravimétrique) et la superficie par BET (Brunauer, Emett et Teller).

Acknowledgment

There are many people I would like to thank for their support, encouragement, and comments over the duration of this project. First and foremost my supervisors, Dr. Arturo Macchi and E.J. Anthony, deserve a great deal of credit for my academic formation. I would like to gratefully acknowledge their support and input.

I would like to show my greatest appreciation to Dr. Firas Ridha for his tremendous support and help. I would like to gratefully acknowledge Dr. Vasilije Manovic for his guidance. I would also like to thank people at CanmetENERGY-Bells Corner Complex for their thoughtful feedback in the team meetings. Thanks are also due to my dear friend, Aida Sharif, who helped me during my studies.

A special thanks to my family. Words cannot express how grateful I am to my mother and father for all of the sacrifices that you have made on my behalf. Your prayer for me was what sustained me thus far. I would also like to thank all of my friends who supported me in writing, and incented me to strive towards my goal. At the end I would like express appreciation to my girlfriend, Mina, for her unflinching support and encouragement throughout my studies.

Table of Contents

List of Tables

List of Figures

Nomenclature

C = Concentration (mol/m^3)

d_p = Particle diameter (m)

D = Column diameter (m)

D_e = Effective Diffusivity (m^2/s)

D_m = Diffusion coefficient (m^2/s)

k = Boltzmann constant (J/K)

K_s = Surface Reaction Constant (m/s)

K_g = External mass transfer coefficient (m/s)

m = mass (g)

n = Number of moles

M = Molecular weight

P = Pressure (atm)

Q = Volumetric flowrate

r_c = Unreacted core radius (m)

R = Particle radius (m)

R = Gas constant

Re = Reynolds number

t = time (s)

T = Temperature

u_t = moving velocity of the transition zone (m/s)

u_g = Superficial velocity of the gas into the reactor (m/s)

X = Fractional conversion

X` = Carbonation conversion

μ = viscosity

η = Adsorption ratio, defined in Equation 4-2

ρ_s = Density (mol/m^3)

τ_{DP} = time (Equation 2-10)

τ_{MT} = time (Equation 2-9)

$\tau_{R,SC}$ = time (Equation 2-11)

ε_{fb} = bed void fraction

Θ = Axial dispersion coefficient

Acronym List

BET = Brunauer-Emmett-Teller

CCS = Carbon Capture and Storage

DAC = Direct Air Capture

GHG = Greenhouse Gasses

GJ = Giga Joule

Gt = Giga Tone

IPCC = International

IEA = International Energy Agency

DEA = Diethanolamine

MEA = Monoethanolamine

OGM = Overlapping Grain Model

ppm = Parts Per Million

RH = Relative Humidity

RPM = Random Pore Model

STP = Standard Pressure and Temperature

TGA = Thermogravimetric Analyzer

XRD = X-Ray Diffraction

Chapter 1

Introduction

1-1 Overview

CO_2 produced by human activities is the main source of greenhouse gasses. The International Panel on Climate Change (IPCC) announced that "*most of the observed increase in globally averaged temperatures since the mid-20th century is very likely due to the observed increase in anthropogenic greenhouse gas concentrations*" [1]. Observations from ice core data in Antarctica show that over the 800000 years preceding industrial era, the CO_2 concentration in the atmosphere had increased from 180 to 270 parts per million (ppm) [2-3]. Measurements from Mauna Loa observatory show that the concentration of CO_2 has increased from ~315 ppm in 1960 to ~400 ppm in 2014 [4].

CO_2 is mostly produced from combustion of fossil fuels such as coal, oil and natural gas. According to the annual report of International Energy Agency (IEA), in 2010 two-thirds of the global CO_2 emissions were from the electricity/heat generation and transport sectors [5].

Carbon Capture and Storage (CCS) is a process of capturing carbon dioxide from large point sources and producing a concentrated and pressurized stream of CO_2 for storage. As is seen in Figure 1-1, CO_2 capture is divided into three different categories: post-combustion, pre-combustion and oxy-fuel combustion. The concentration of CO_2 in

the gas stream, the pressure of the gas stream and the fuel type (solid or gas) are important factors in selecting the capture system. The most well-known approach for CO_2 capture is via post-combustion. It has been used in power plants to remove CO_2 from flue gas for many years. Moreover, acid gas removal from natural gas uses similar technology. Pre-combustion capture is mostly applied in hydrogen production. Although the initial fuel conversion steps of pre-combustion are more elaborate and costly, the higher concentrations of CO_2 in the gas stream and the higher pressure make the separation easier. Oxyfuel combustion, which is under development, uses high purity oxygen. Hence, high CO_2 concentrations in the gas stream and easier separation of CO_2 will be achieved but energy is required for the separation of oxygen from air [6]. However, despite the focus on large point sources, about 60% of CO_2 emission is attributed to dilute sources [8].

Direct Air Capture (DAC) is a developing technology for removing carbon dioxide from the atmosphere. Unlike other CO_2 removal processes, it does not need a concentrated source of CO_2, and hence could be used in CO_2 treatment of power generation plants to oil and gas refineries to enhanced oil recovery.

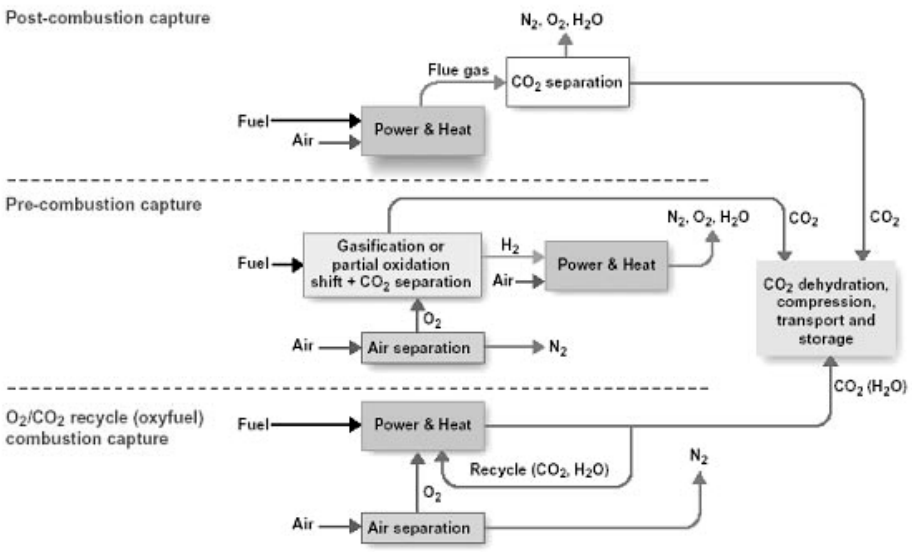

Figure 1-1 Schematic representation of CO_2 capture systems [6]

1-2 Thesis objectives and organization

The purpose of this thesis is to study the performance of two different lime-based sorbents for CO_2 capture from dilute sources. This goal will be achieved by investigating CO_2 breakthrough curves of both sorbents under different operating conditions: flowrate (0.26 L/min and 0.53 L/min at 1 barg and 20 °C), particle size (250-425 µm and 425-600 µm) and relative humidity (55% and 78%). Their CO_2 capture capacity will be measured and compared in a series of carbonation/calcination cycles. Finally, a gas-solid reaction model will be used to quantify the kinetics of the reaction for both sorbents.

This thesis has five chapters. Chapter 1, Introduction, presents the rational and objective of this project. Chapter 2, Background and Literature Review, discusses some of technologies for CO_2 removal from air and the current research theories. Chapter 3,

Experimental Methods, introduces the experimental setup, methods for preparation of the samples and analysis of the CO_2 concentration in order to determine the breakthrough curves. Procedures for determining the carbonation conversion and pore surface area will also be discussed in this chapter. Chapter 4, Results and Discussions, focuses on the effects on the breakthrough curves of changing the operating conditions and the mathematical model proposed to analyze data from breakthrough curves. The effects of the carbonation/calcination cycles on the carbonation conversion and pore surface area for both sorbents will also be studied in this chapter. Finally, chapter 5, Conclusions and Recommendations, summarizes conclusions drawn and presents suggestions and directions for further developments.

Chapter 2

Background and Literature Review

It has been widely proposed that anthropogenic emission of greenhouse gases (GHG) has a significant effect on climate change due to global warming [5, 7, and 8]. Since fossil fuels are still the least expensive source of energy, it is predicted that GHG emissions due to combustion of fossil fuels will rise by 25-90% between 2000 and 2030 [9]. Figure 2-1 shows that CO_2 emission from industries and power plants is less than 50% of the world CO_2 emissions and more than 60% of CO_2 emissions are from dilute sources [8]. Moreover, distributed carbon dioxide sources account for approximately half of the total emissions [10]. Unfortunately, although oceans absorb most of the emitted CO_2, 20-40% of it remains in the atmosphere [11].

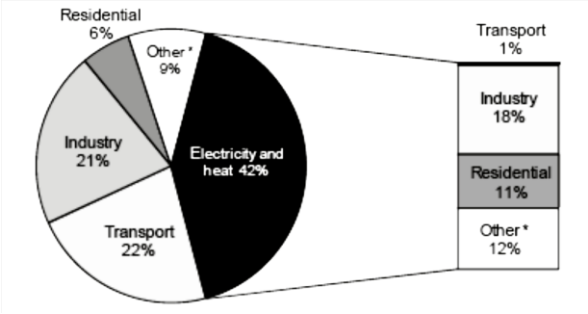

Figure 2-1 World CO_2 emissions by sector in 2011 [8]

Carbon Capture and Storage (CCS) is a proposed approach to separate CO_2 from combustion flue gases and inject it underground [12]. It is thus being developed for power

generation and large industries. Direct capture of CO_2 from ambient air (air capture) is a developing technology, which is capable of removing CO_2 directly from the atmosphere [12]. Most proposed processes of CO_2 capture from air can be built wherever the nearly pure stream of CO_2 is needed. This makes it unique in comparison with other CO_2 capture processes where a high CO_2 concentration source is needed.

The change of the Gibbs free energy for air capture is relatively higher than CO_2 capture from typical industrial CO_2 sources. Moreover, direct air capture is kinetically slow at ambient conditions (low temperature and low CO_2 concentration). Hence, in overall, CO_2 capture from air is not favorable [14]. Capturing CO_2 with a partial pressure p_0 from a mixture of gases and separating it as a pure CO_2 stream with a pressure p, needs $kTln(p/p_0)$ energy, where k and T are the Boltzman constant and working temperature, respectively. Therefore, capturing CO_2 (partial pressure ~4×10^{-4} atm) from air and compressing it to 100 atm in pressure, which is required for sequestration, needs an energy input of almost 4 GJ per ton of carbon. Comparing the value of 4 GJ/tone of carbon to the carbon-specific energy content of fossil fuels, such as coal, oil and natural gas (40-70 GJ/tone of Carbon), suggests that part of the energy from these carbon fuels can be used for CO_2 capture rather than being emitted to the atmosphere [13]. Moreover, the environmental advantages of CO_2 capture from air are undeniable. For instance, CO_2 capture sites could be constructed next to the final storage sites such as deserts , in which the land is cheap, energy for the separation process can be generated from renewable energies (wind or solar), and no cost of transportation is required. They could also be

located next to the tailing CO_2 treatment of power generation plants or oil and gas refineries, where 100% CO_2 capture from their sources is not achieved [8,14].

2-1 Wet Air Capture System

One of the most well-known methods for "direct air capture" is using hydroxide solutions. This method is being further developed and currently a pilot plant of this process is operated by Carbon Engineering Ltd in Calgary, Canada [15]. The schematic of the process is shown in Figure 2-2. Although it has several steps, the process mainly consists of 2 cycles: an air contactor (CO_2 capture cycle) and a sorbent regeneration cycle. Working together, these two cycles continuously capture CO_2 from air. While small amounts of make-up chemicals and energy are input into the process, nearly pure CO_2 is an output. As mentioned, this CO_2 can be used as a chemical for industrial purposes, or can be stored permanently [13].

In the first stage, CO_2 from air is absorbed by means of a chemical solution. Captured CO_2 from the air contactor is in a carbonate format (usually K_2CO_3). The carbonate solution then reacts with a hydroxide (usually calcium hydroxide) and forms $CaCO_3$.

In the next stage, solid calcium carbonate is separated from the solution and calcined to CaO in a fluidized bed that operates at approximately 900 °C. During this stage, CO_2 is released as a gas. The calciner works in oxy-fuel mode where the fuel, such as natural gas, burns in an environment without nitrogen producing a flue gas consisting

primarily of CO_2 and water vapor which can be condensed to leave a stream of nearly pure CO_2 ready for compression. CO_2 free CaO solids are then sent to a tank to become hydrated and form $Ca(OH)_2$. This hydroxide will be used to react with the carbonate solution [12 and 15].

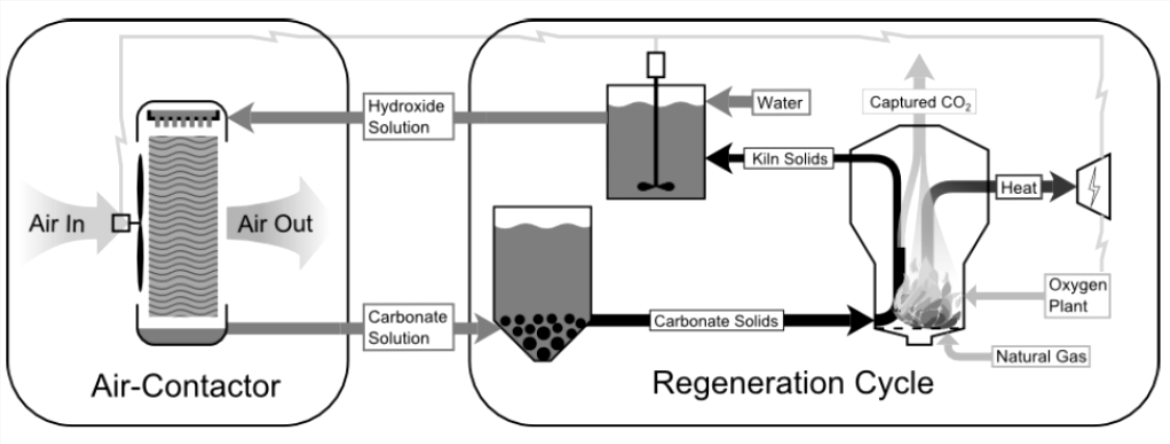

Figure 2-2 Schematic of the wet scrubbing method [15]

Recently, systems using NaOH in the contactor have become of interest. Since the process uses a liquid solution, good contact between the liquid and ambient air is critical. Among the suggested solutions for this challenge, a spray-based system and a packed tower have been tried [16]. However, these methods have some drawbacks, such as, high cost of sorbent regeneration, solvent loss, and sodium salt impurities in the calcium loop that contributes to the sintering and loss of sorption capacity.

2-2 Carbon Dioxide Capture via Plants (forestry)

The important role of forests in CO_2 capture is undeniable. Most of the carbon dioxide emissions from land use change are attributed to deforestation. Studies show that the annual emission of CO_2 due to the deforestation is 1.2 to 1.9 Gt C [17].

CO_2 capture via plants is based upon capturing CO_2 by recovering the vegetation of a degraded area or planting in a renewable cycle. It is also suggested that biomass product of mature forests can be used as fuel. In many countries, short and long rotation forestry is being used where rotation of growth and harvest is from 6 to 60 years (short rotation) or from 20 to 100 years (long rotation). Since deforestation is known as the second most important source of GHG emissions, this method can also make up the CO_2 emission due to deforestation. Moreover, supporters of this method also suggest that conservational activities to avoid deforestation are necessary [18 and 19].

Maintenance of the recovered forest to keep the carbon stored for long periods of time is one of the main uncertainties of this technology. Another is the competition for land in the future for other human needs [19]. Moreover, unlike other CO_2 capture systems from air, using biomass for air capture is limited by the availability of biomass [13].

It could therefore be suggested that forestry should be pursued in the short-term before land prices significantly increase [17].

2-3 Amine Based Sorbents for CO_2 capture from Air

Amine scrubbing is a mature technology which has been used for more than 60 years in oil and gas industries for acid gas (H_2S and CO_2) removal. Amine-based solutions are the most well-known solvents for CO_2 removal from industrial source. However, for direct air capture, solutions such as Diethanoleamine (DEA) and Monoethanoleamine (MEA) are not suitable since their CO_2 capture capacity drops drastically at low partial

pressure of CO_2. Amine-based solid sorbents can be used instead. Supported amine adsorbents are divided into 3 categories:

In class 1 adsorbents, amine molecules are loaded in polymeric or silica supports. These amine molecules are physisorbed on the surface or in the pores of the support. Unlike class 1, in class 2 adsorbents, amine molecules are bound to the surface of the support by covalent bounds. Studies show that class 2 adsorbents have better performance than other adsorbents such as zeolites and mesoporous silica at low CO_2 partial pressure [20].

Recently, a new class of amine-based solid adsorbents has been introduced in which the materials are covalently bound polymeric amines in porous layers. This new class of adsorbent shows outstanding performance compared to class 1 and class 2 adsorbents.

Despite the low regeneration cost of amine-based adsorbents which makes them favorable for direct air capture, their operational costs, poor CO_2 capture capacity from air (where partial pressure of CO_2 is too low), and degradation are some of the issues that make them less attractive options [20 and 21].

2-4 Carbon Dioxide Capture via Lime-Based Sorbents

CO_2 capture at high temperature via new lime-based sorbents, which are enhanced with binders by means of pelletization, has been recently investigated by CanmetENERGY-Ottawa. Results show improved sorption capacity relative to natural limestone [22-24]. Since research and experiments on capturing CO_2 were for highly concentrated sources at elevated temperatures, this new sorbent has become a material of interest for more applications.

Pellets are made with a mechanical pelletizer (Glatt GmbH). First, powdered calcined sorbents (CaO) which are fine particles <45 μm and calcium aluminate cement (CA-14) with composition of ~71% Al_2O_3, ~28% CaO, and ~1% Impurities; with a ratio of 9/1 by mass are mixed in the pelletization vessel. Then, water is sprayed into the vessel continuously. The size of the pellets is controlled by the speed of an agitator and chopper, which are attached to the vessel. The schematic of the pelletizer is shown in Figure 2-3.

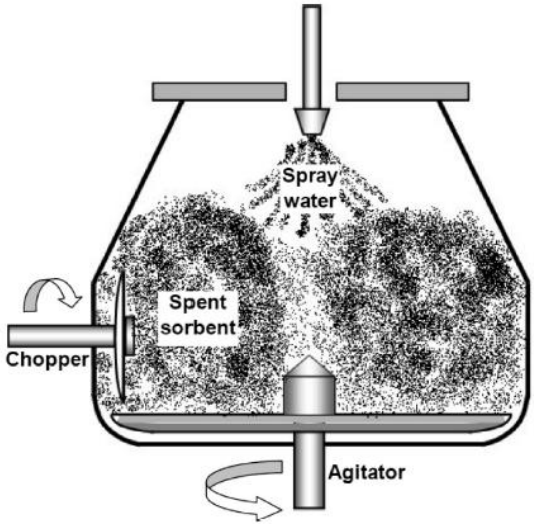

Figure 2-4 Schematic of the pelletizer vessel [24]

The superior performance of the pelletized limestone in carbonation-calcination cycles is due to the formation of mayenite ($Ca_{12}Al_{14}O_{13}$). This compound provides nanosized structures which reduces sintering upon calcination [22-25].

Significant carbonation of calcium hydroxide at ambient temperature can be achieved with the relative humidity (RH) of air is above 40% [26]. Dheilly *et al.* suggest that it is not the CO_2 partial pressure, but H_2O partial pressure which dominates the carbonation reaction at low temperature [27]. Furthermore, observations of Yang et al

[30] via an atomic force microscopy (AFM) confirms that the carbonation of calcium hydroxide at ambient conditions occurs when nano-droplets of water on the surface of $Ca(OH)_2$ are formed. The carbonation of lime occurs in several steps [28] that are suggested based on the prior observations. First, nano-droplets of water on the surface of the sorbents are formed (Figure 2-5). Then, Figure 2-6 shows that gaseous CO_2 will dissolve in those water droplets and forms H_2CO_3 (equation 2-2); at the same time, calcium hydroxide from the surface of the sorbent is dissolved in the water. While H_2CO_3 dissociates to its H^+ and CO_3^- ions (equations 2-3 and 2-4), $Ca(OH)_2$ dissociates to its Ca^{2+} and OH^- ions (equation 2-1).

$$Ca(OH)_2 \leftrightarrow Ca^{2+} + 2OH^-_{(aq)} \qquad \text{Equation 2-1}$$

$$CO_2 + H_2O \leftrightarrow H_2CO_{3\,(aq)} \qquad \text{Equation 2-2}$$

$$H_2CO_3 \leftrightarrow HCO_3^-{}_{(aq)} + H^+_{(aq)} \qquad \text{Equation 2-3}$$

$$HCO_3^-\,(aq) \leftrightarrow CO_3^{2-}{}_{(aq)} + H^+_{(aq)} \qquad \text{Equation 2-4}$$

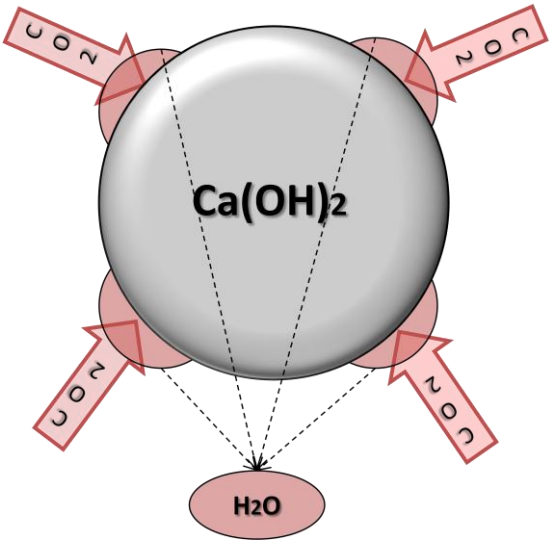

Figure 2-4 Formation of nano-droplets of water on the surface of $Ca(OH)_2$

And the overall carbonation reaction of $Ca(OH)_2$ would be written as:

$$Ca(OH)_2 + CO_2 + H_2O \leftrightarrow CaCO_3 + H_2O \qquad \text{Equation 2-5}$$

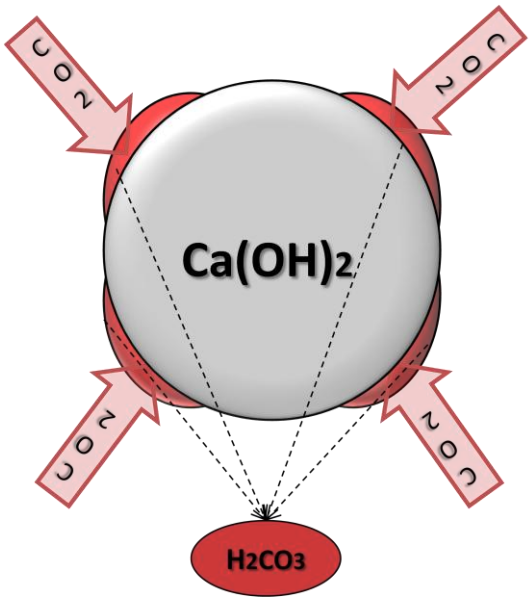

Figure 2-5 Formation of H_2CO_3 on the surface of the sorbent

Since studies show high carbonation conversion of $Ca(OH)_2$ at ambient conditions, it can be concluded that the new solid phase on the surface of the particles is non-protective [26]. This can be explained due to the formation of calcium bicarbonate by the following reaction [29]:

$$CaCO_3 + CO_2 + H_2O \rightarrow Ca(HCO_3)_2 \qquad \text{Equation 2-6}$$

Higher solubility of calcium bicarbonate enhances CO_2 diffusion through the bulk of the particle. Finally, calcium bicarbonate reacts with $Ca(OH)_2$ and forms calcium carbonate:

$$Ca(HCO_3)_2 + Ca(OH)_2 \rightarrow 2CaCO_3 + 2H_2O \qquad \text{Equation 2-7}$$

Since these reactions (Equations 2-5 and 2-7) are occurring in parallel, for simplification of mathematical modeling they are considered as one reaction and the new phase solid layer will be considered as a non-protective layer.

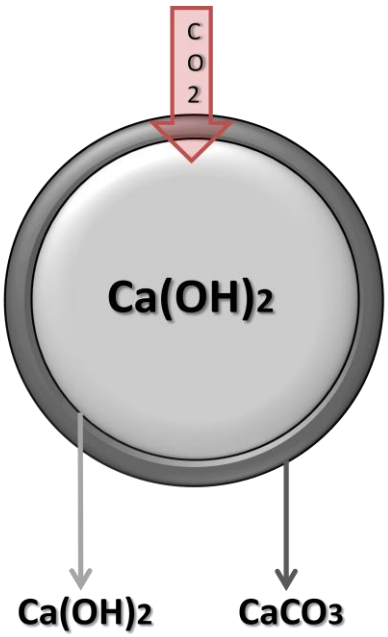

Figure 2-6 $CaCO_3$ layer on the surface of the sorbent

Since the solubility of gases is greater at low temperatures than at high temperatures, the carbonation of $Ca(OH)_2$ at a lower temperature (*i.e.* 10 °C) is greater than at a higher temperature (*i.e.* 40 °C) [27 and 29].

After the formation of the $CaCO_3$ layer on the surface of the particles (Figure 2-7), due to the difficulty of CO_2 diffusion through the product layer; further reaction between CO_2 and the reacting particle will become slow [29].

2-5 Modeling of non-catalytic gas-solid reaction

Nikulshina *et al.* [31] have shown that kinetics of the reaction between CO_2 and $Ca(OH)_2$ is much faster than the reaction of CO_2 and CaO when the concentration of CO_2 is low (500 ppm) and the temperature is between 300 and 400 °C. The study was performed using fine powders (particles with an average diameter of ~ 50 μm) of CaO and $Ca(OH)_2$. The study also shows that carbonation of CaO in the presence of water vapor (50% H_2O) is 22 and nine times faster than carbonation of calcium oxide and calcium hydroxide, respectively, in a dry system. Moreover, the reaction of CaO and CO_2 at the conditions of the experiments has 2 different rate-limiting regions: reaction-controlled and diffusion-controlled. However, the carbonation of $Ca(OH)_2$ at temperatures above 300 °C is dominated by the chemical reaction and the resistance of the product layer $CaCO_3$ is not noticeable at those temperatures and short diffusion lengths. The model which was used to fit the carbonation of $Ca(OH)_2$ was primarily based on the solid specific surface area, temperature and relative humidity [32]. The model assumes that the carbonation of lime is controlled by surface reaction and the reaction occurs only on reactive areas on the surface which are not carbonated and covered by protective layer. The model assumes that the carbonation of lime is controlled by surface reaction and the reaction occurs only on reactive areas on the surface which are not carbonated and covered by protective layer.

The effect of steam on the carbonation rates of CaO at 650 °C shows that the steam elevates the carbonation conversion when the kinetics of the reaction is controlled by diffusion through the product layer [33 and 34].

The carbonation kinetics of a CaO-based sorbent (which was enhanced by $Ca_9Al_6O_{18}$) was studied by Zhou *et al.* [35]. They used the Random Pore Model (RPM) and the Overlapping Grain Model (OGM) to study the kinetics of the carbonation of the CaO-based sorbent at temperatures ranging from 500 °C to 700 °C and to compare results from each model. Although both models fit the experimental data, results obtained for the surface reaction constant and effective diffusivity were not similar. The difference comes from the methods the models use to handle the carbonation conversion curve. In the RPM model, the conversion curve is divided into two regions: the reaction-controlled region and the product layer diffusion-controlled region. In the reaction-controlled region, the effect of diffusion is not considered and in the diffusion-controlled region, the effect of the chemical reaction is not considered. In the OGM model, the conversion curve is treated as a whole and both reaction and diffusion are considered at the same time.

Based on different steps of the carbonation reaction, it can be assumed that the reaction of calcium hydroxide and CO_2 is a non-catalytic, gas-solid reaction. Among these groups of reactions, the unreacted shrinking core model is one of the simplest models as it does not require specific knowledge of the internal structure of the reacting solid.

This model consists of 3 major steps:

- Diffusion of the gaseous reactant (CO_2) through the gaseous film surrounding the particle to the surface of the solid ($Ca(OH)_2$).

- Diffusion of the gaseous reactant through the product layer to the unreacted core.

- Reaction of the gaseous reactant with the solid at this reaction surface.

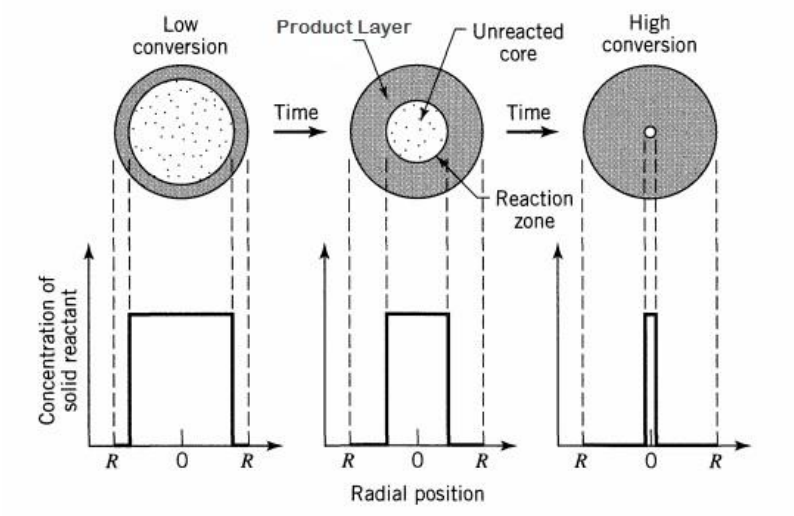

Figure 2-7 Conversion of the particle based on the unreacted core model [36]

In this research, the reaction part of the model includes all reactions which were introduced before (Equations 2-1 to 2-7). Moreover, as explained in section 2-4, formation of the $Ca(HCO_3)_2$ on the product layer of the sorbent, makes the diffusion of CO_2 to the bulk of the particle easier. However, continued formation of $CaCO_3$ impedes further CO_2 diffusion.

The model gives the time necessary to reach a given conversion of the solid, based on the following equations [36]:

$aA_{(g)} + bB_{(s)} \rightarrow rR_{(g)} + sS_{(s)}$ Equation 2-8

$t/\tau_{MT} = X_B$ Equation 2-9

and $\tau_{MT} = \frac{\rho_B R}{3bK_g C_{Ag}}$

$t/\tau_{DP} = 1 - 3(1-X_B)^{2/3} + 2(1-X_B)$ Equation 2-10

and $\tau_{DP} = \frac{\rho_B R^2}{6bD_e C_{Ag}}$

$t/\tau_{R,SC} = 1-(1-X_B)^{1/3}$ Equation 2-11

and $\tau_{R,SC} = \frac{\rho_B R}{bk_s C_{Ag}}$

where τ_{DP} is the characteristic time for diffusion of the gaseous reactant through the product layer of the particles, τ_{MT} is the characteristic time for external mass transfer from the bulk gas to the surface of the particle, and $\tau_{R,SC}$ is the characteristic time for chemical reaction at the interface between the unreacted core of the pellet and the reacted product layer and X is the fractional conversion which is defined as:

$X_B = 1 - (\frac{r_c}{R})^3$ Equation 2-12

Chapter 3

Experimental methods

This chapter describes the experimental material, set-up, procedure, and analysis of the effluent gas from the fixed-bed. The experimental parameters are type of sorbent (Pelletized Limestone and Natural Limestone from Cadomine), particle size (250-425 µm and 425-600 µm in diameter), volumetric flowrate (0.5 L/min and 1 L/min at STP conditions) and relative humidity (55% and 78%).

3-1 Materials

The composition of natural limestone which was measured by X-Ray Diffraction (XRD) analysis can be found in Table 3-1.

The pelletized sorbents contain 10% binder (calcium aluminum cement-CA 14) and 90% natural limestone (same limestone as in Table 3-1). As mentioned in chapter 2, the binder not only improves the physical strength of the sorbents, but it increases their average surface area.

Table 3-2 shows some physical properties of natural and pelletized limestone. Natural limestone has greater bulk density, while pellets have greater surface area. The difference comes from the binder, which via formation of mayenite enhances the surface area of the sorbents and decreases the density.

Table 3-1 Composition of Natural Limestone

Component	Wt%
CaO	89.57
SiO_2	4.03
MgO	3.92
Al_2O_3	1.06
Fe_2O_3	0.51
K_2O	0.38
Na_2O	0.35
SO_3	0.17
TiO_2,P_2O_5,Br,Ni,Mn,Zn,Cu	0.01
Total	100

Table 3-2 Some physical properties of sorbents

	Pellets (250-425 μm)	**Pellets (425-600 μm)**	**Natural Limestone (250-425 μm)**	**Natural Limestone (425-600 μm)**
Bulk Density (g/cm^3)	0.87	0.84	0.98	0.96
Surface Area (m^2/g)	14.61	12.01	13.60	11.54

Before each experiment pelletized limestone and natural limestone are pre hydrated for approximately 3 hours by passing nitrogen through the bubbler and then the fixed bed. Hence, particles, which mostly contain calcium oxide, react with water vapor and the bed is eventually converted to calcium hydroxide.

$$CaO_{(s)} + H_2O_{(g)} \rightarrow Ca(OH)_{2(s)} \qquad \text{Equation 3-1}$$

3-2 Designing the experimental set up

The schematic of the experimental set up is shown in Figure 3-1. A compressor is used to circulate air from the atmosphere (outside the laboratory) through a bubbler to become humidified and then through a packed bed of sorbents. The average CO_2 concentration of air is 415 ppm. Then, relative humidity at the outlet of the bubbler is measured by a Vaisala RH-Transmitter while a rotameter measures the gas flow rate.

The column containing the bed of particles is a stainless steel tube with a height of 78.57 mm and inner diameter of 7.80 mm. The schematic of the reactor is shown in Figure 3-1.

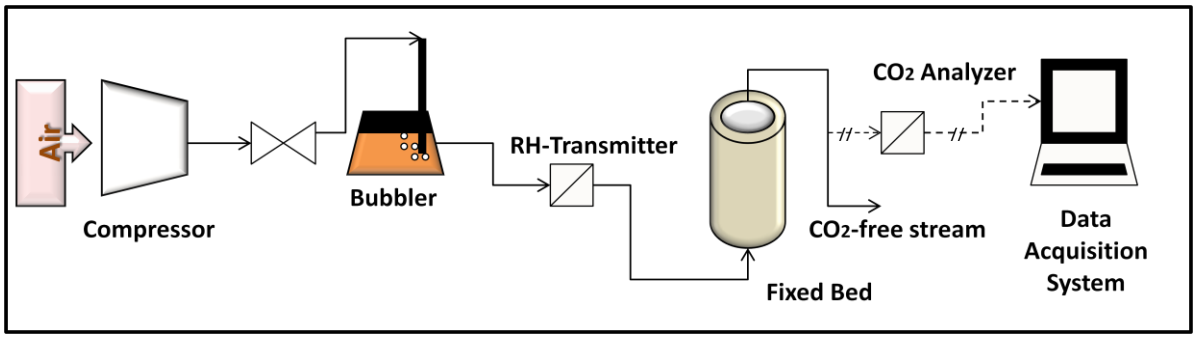

Figure 3-1 Experimental set up

When designing fixed bed reactors, several parameters should be considered such as the length of the packed column, the ratio of the column to particle diameter (D/d_p)

and the ratio of column length to diameter. It has been shown that in fixed beds with $D/d_p>15$, a flat velocity profile and uniform porosity can be assumed [37 and 38]. Other studies have shown that this assumption is also valid with $D/d_p>10$ [39 and 40].

Moreover, under similar conditions, values of the gas axial dispersion coefficient measured at different column lengths, should be similar. The axial dispersion coefficient for uniform packed beds is constant under the following condition [41]:

$$\Theta = \frac{D_m t}{d_p^2} \geq 0.15 \qquad \text{Equation 3-2}$$

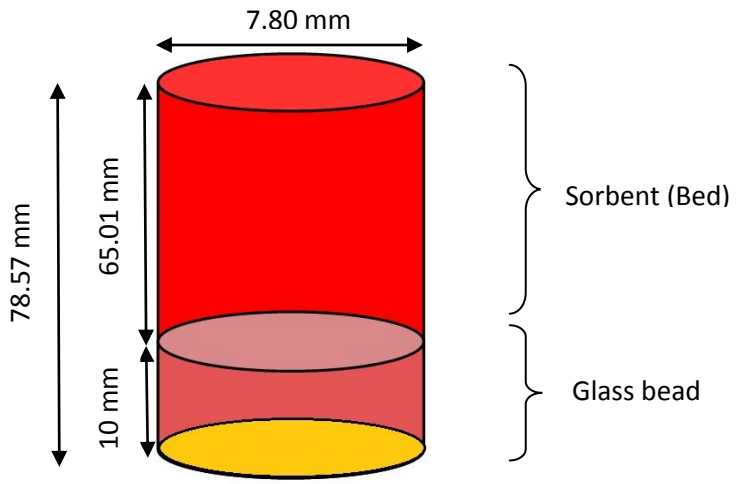

Figure 3-2 Layout of the Reactor

in which, d_p and D_m are the average particle diameter and molecular diffusion coefficient respectively, and t is time.

In another study, Taylor [42] has shown that the axial dispersion coefficient is constant if:

$\Theta = \frac{D_m t}{D^2} >> 0.14$ Equation 3-3

In which, D is column radius.

In another study, Ribeiro *et al.* show that the average bed porosity in a packed bed tends to ~ 0.35 when D/d_p is greater than 15 [43].

Based on the above studies and considering the range of particle diameter for this study (250-600 µm), a fixed bed with the following dimensions was designed:

L = 65.01 mm

D = 7.80 mm

Minimum of D/d_p (based on the largest particle) = 15.2195

$\Theta_{minimum}$ (based on Equation 3-3) = 1.08

To minimize fluid channeling, the column lower section contains glass beads of 200-300 µm in diameter filled to 1 cm high. A paper filter with pore size of 8 µm was also inserted at the bottom of the column.

Flowrates were chosen to ensure that, based on the Reynolds number, the flow regime remained constant in all experiments. The particle Reynolds number defined in equation 3.4 varied between 0.37 and 1.12, below the upper limit value of 10 for laminar flow [44].

$Re = \frac{\rho V_s d_p}{\mu(1-\varepsilon)}$ Equation 3-4

In order to make sure that the carbonation conversion throughout the entire bed was uniform, after a complete breakthrough, the conversion of sorbents was determined by a thermogravimetric analysis (TGA) with a METLER TOLEDO-SDTA581 (Figure 3-3). Sample sorbents were selected from the top, middle and bottom of the bed.

Figure 3-3 Thermogravimetric Analyzer - METLER TOLEDO-SDTA581

Natural limestone and pelletized limestone sorbents with particle size range of 425-600 μm were used to investigate their performance in a series of carbonation/calcination cycles. Nine cycles which consisted of CO_2 capture from air at ambient conditions (carbonation) and regeneration of sorbents (calcination) at 850 °C in air for 75 minutes were conducted.

Figure 3-4 BET - Micromeritics-TriStar II

After each carbonation period (at the end of the breakthrough), the carbonation conversion of sorbents was examined by a TGA Subsequently, after calcination of sorbents, their surface area was measured by a BET (Brunauer–Emmett–Teller) with a (Micromeritics-TriStar II).

Chapter 4

Experimental Results and Discussion

This chapter describes and discusses the results obtained from different experimental studies. First, in section 4-1 reproducibility of the data with set-up and procedure will be presented. The necessity of moisture and pre-hydration will be examined in section 4-2. In section 4-3, the effects of particle size, flowrate and particle type on CO_2 capture from air at ambient conditions will be presented. Section 4-4 will discuss the effect of relative humidity on air capture. While in sections 4-5 and 4-6 will present the performance of the sorbents in the series of capture and regeneration cycles. Finally, in section 4-7, the data will be fitted to a suitable non-catalytic gas solid reaction model in order to quantify results from previous sections.

4-1 Reproducibility of data

The reproducibility of data with an experimental setup and procedures is critical to the accuracy of research. Therefore, three experiments were performed at the same conditions: sorbent loading ~ 2.10 g natural limestone, gas flowrate of 0.26 L/min at 1 barg and 20 °C; and particle size range of 250-425 µm. Particles were pre hydrated for approximately 3 hours and the relative humidity was ~55% during each run. As mentioned in chapter 3, the average concentration of air is 415 ppm. In this work, uncertainties were analyzed by using the Student t test at the 95% probability level. (Figure 4-1 shows the

breakthrough curves of the three runs of experiments). For all runs, the breakthrough point is defined as $C/C_0 = 0.1$.

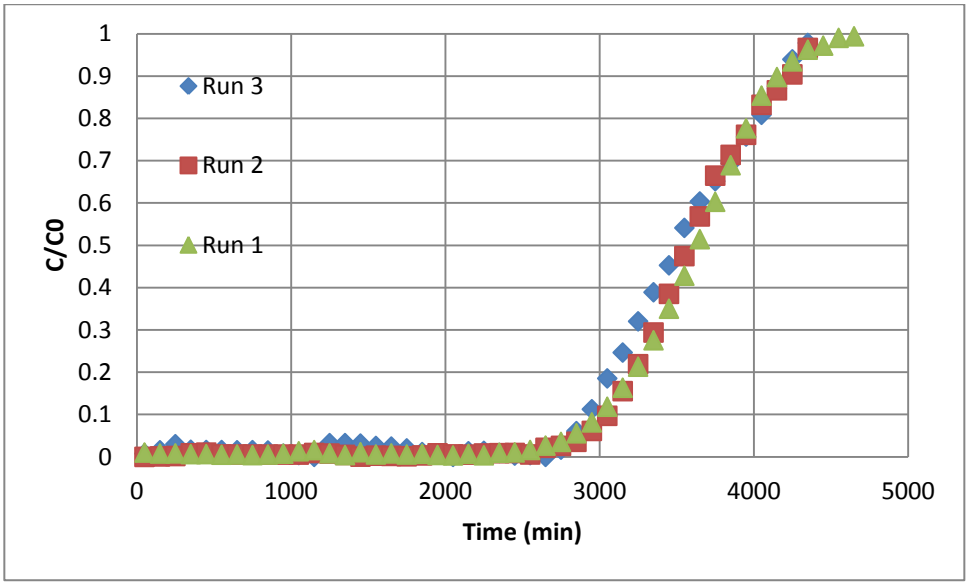

Figure 4-1 Reproducibly of data: CO_2 capture Prehydrated Natural Limestone-250-425 µm-0.53 LPM (1 barg, 20 °C)

Table 4-1 Loading and breakthrough time of natural limestone for three runs

Run Number	1	2	3
Sorbent Loading (g)	2.1035	2.1055	2.0985
Average Sorbent Loading (g)	2.1025		
Breakthrough Time (min)	2840	2890	2770
Coefficient of variations	0.1715		

4-2 Necessity of Moisture

As mentioned in chapter 2, almost no carbonation reaction occurs when there is no humidity in the fixed bed system [26-28 and 31]. From Figures 4-2, 4-3, 4-4 and 4-5, although samples are prehydrated for almost 3 hours, in the absence of humid air not only was the breakthrough time short (Figures 4-2 and 4-4), but the carbonation of the sorbents was low (less than 10% - Figures 4-3 and 4-5). However, if the inlet stream (air) is humidified up to 50-55% relative humidity, but sorbents are not pre-hydrated, a non-uniform carbonated bed is observed (Figures 4-7-a and 4-7-b). This phenomenon is due to the partial carbonation of sorbents in the first layers of the bed. While there is a competition between CO_2 and water to react with CaO, partial carbonation reaction on the surface of the sorbents not only prevents further hydration, but also decreases the reaction rate at the surface. However, in comparison with a dry system where relative humidity was negligible and sorbents were not pre-hydrated, the observed carbonation conversion was higher.

The carbonation conversion is defined in equation 4-1:

$$\text{Carbonation Conversion (X')} = \frac{m_2 - m_1}{A \times m_0} \times \frac{M_{CaO}}{M_{CO_2}} \qquad \text{Equation 4-1}$$

where, m_2 and m_1 are respectively the mass of carbonated and calcined sample; m_0 is the initial mass of the sample and A is the fraction of CaO in the sorbent. M_{CaO} and M_{CO_2} are molecular weight of calcium oxide and carbon dioxide respectively.

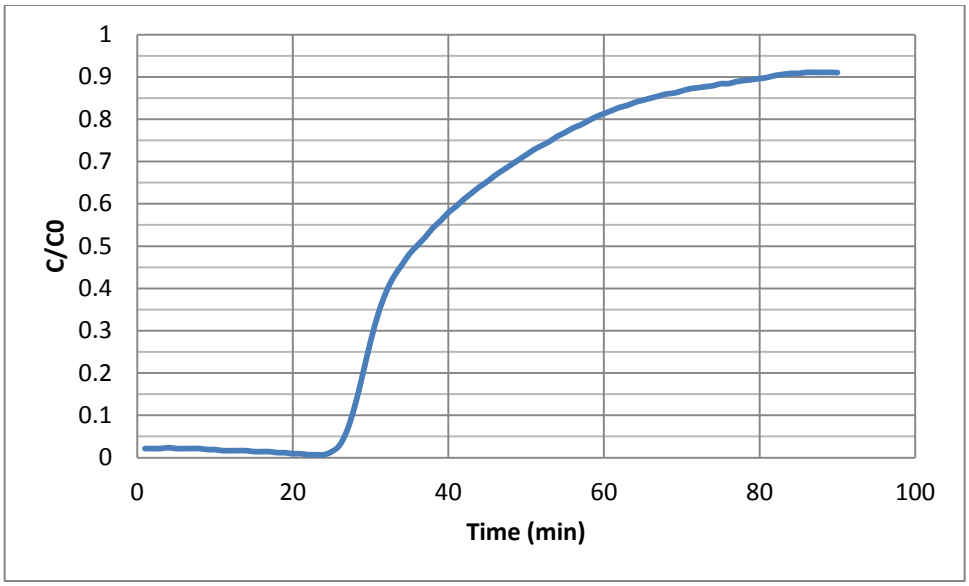

Figure 4-2 Breakthrough curve - dry system (RH~0%) – Prehydrated *Natural limestone*-250-425 µm-0.53 LPM (1 barg, 20 °C)

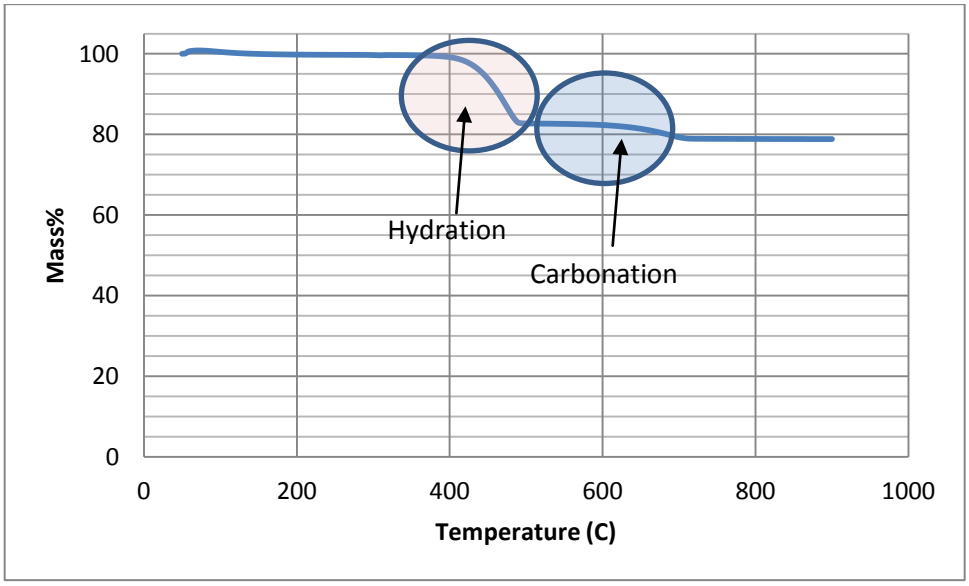

Figure 4-3 Hydration and Carbonation conversion of Prehydrated *Natural Limestone* - dry system (RH~0%) - 250-425 µm - 0.53 LPM (1 barg, 20 °C)

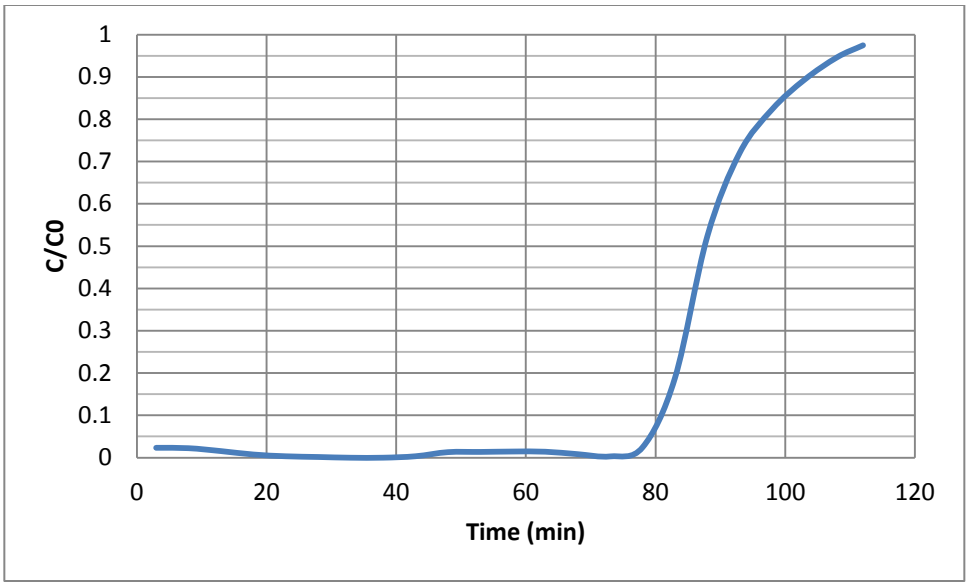

Figure 4-4 Breakthrough curve - dry system (RH~0%) - Prehydrated *Pelletized limestone*-250-425 µm-0.53 LPM (1 barg, 20 °C)

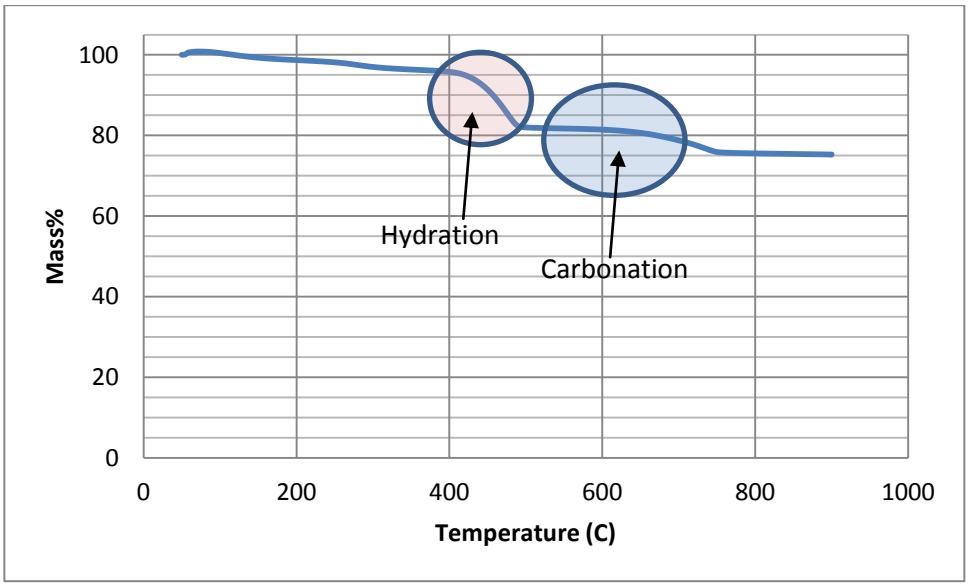

Figure 4-5 Hydration and Carbonation conversion of Prehydrated *Pelletized Limestone* - dry system (RH~0%) - 250-425 µm-0.53 LPM (1 barg, 20 °C)

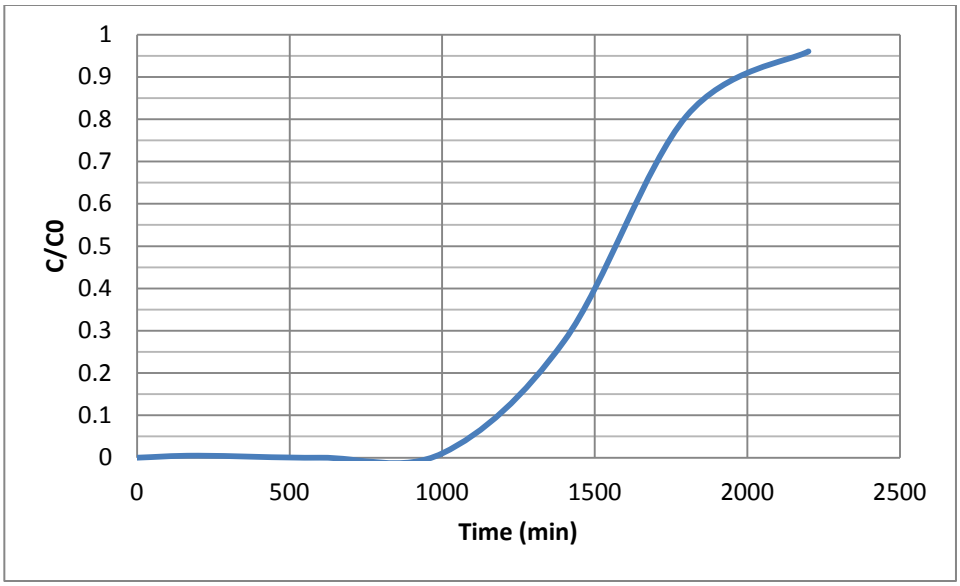

Figure 4-6 Breakthrough curve – humidified system (RH~55%) - Pelletized Limestone - *without pre-hydration* - 425-600 µm-0.53 LPM (1 barg, 20 °C)

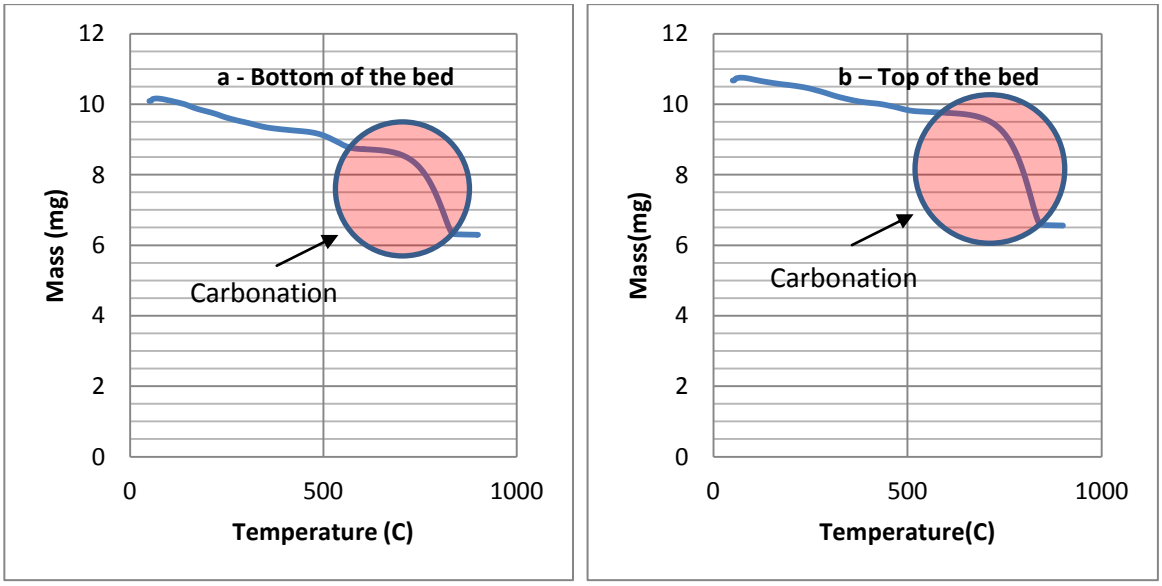

Figure 4-7 Hydration and Carbonation conversion of Pelletized Limestone - (a-bottom of the bed) - (b-top of the bed) without pre-hydration - humidified system (RH~55%) - 425-600 µm-0.53 LPM (1 barg, 20 °C)

Hence, in order to have a uniformly carbonated bed after a complete breakthrough, all sorbents are pre-hydrated for approximately 3 hours producing a

reactive $Ca(OH)_2$. At the same time, air is being moisturized (RH~55%) to enhance the carbonation reaction.

4-3- Effect of Particle Size and Flow Rate:

4-3-1-Pelletized Limestone:

As explained in chapter 3, in order to minimize the effect of the mass transfer from the bulk to the surface of the particles, gas flowrates are set to a range between 0.26 L/min and 0.53 Lit/min at 1 barg, 20 °C (0.5 L/min and 1 L/min at STP conditions).

Figure 4-8 shows the effect of changing particle size and gas flow rate on the breakthrough time and breakthrough curve. It can be seen that smaller particles have a better performance (steeper breakthrough slope) due to their higher pore surface area. Hence, their overall CO_2 capture in comparison with larger particles is better.

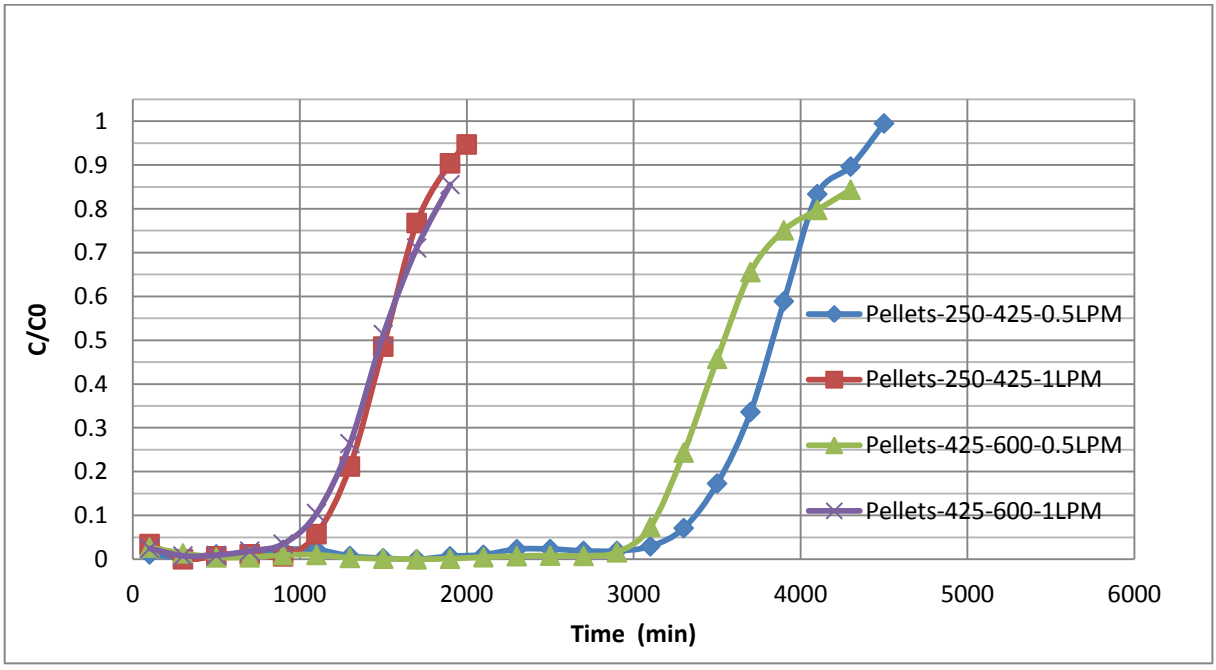

Figure 4-8 Effect of Particle size and gas flowrate on the breakthrough curve (Pelletized Limestone)

As the slopes of the breakthrough curves are similar for different flowrates, external mass transfer from bulk to the surface of the pelletized limestone particles is as expected, negligible.

In order to confirm recorded data from the breakthrough curves and TGA, a mass balance in the gas phase was used and results from both methods were compared in Table 4-2, which shows that the difference between carbonation conversion obtained from the TGA and calculated from mass balance (based on Equation 4-2) is negligible. Figure 4-9 show a uniform carbonation conversion along the bed in a selected run. This uniform carbonation conversion along the bed, confirms our previous statement about the necessity of moisture and pre-hydration.

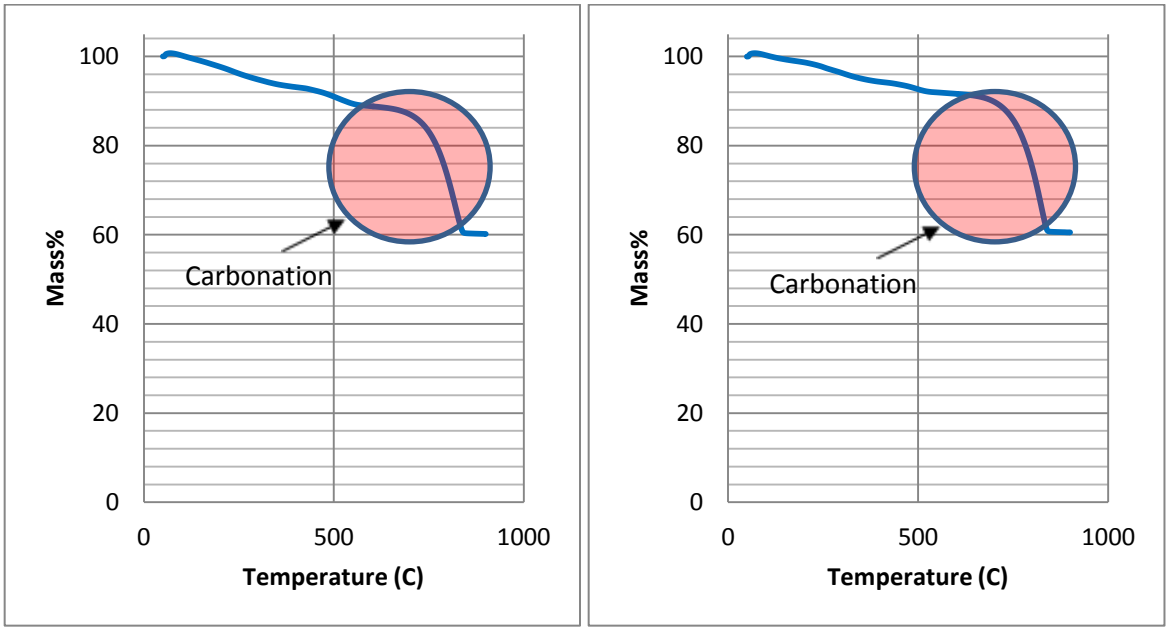

Figure 4-9 Hydration and Carbonation conversion of Pre hydrated Pelletized Limestone - (a-bottom of the bed) - (b-top of the bed) - humidified system (RH~55%) - 425-600 µm-0.53 LPM (1 barg, 20 °C)

As mentioned before, CO_2 Mass balance is calculated by the following equation:

$$n = [CO_2]_{in} \times Time \times \frac{P \times Q \times \eta}{R \times T}$$ Equation 4-2

where n is the number of CO_2 moles that are adsorbed in the bed, P is the pressure of the system, Q is volumetric flowrate, R is the ideal gasses constant, η is the ratio of the area above the breakthrough curve to the whole area as shown in Figure 4-10 ($\eta = \frac{P}{1 \times t}$), and T is temperature.

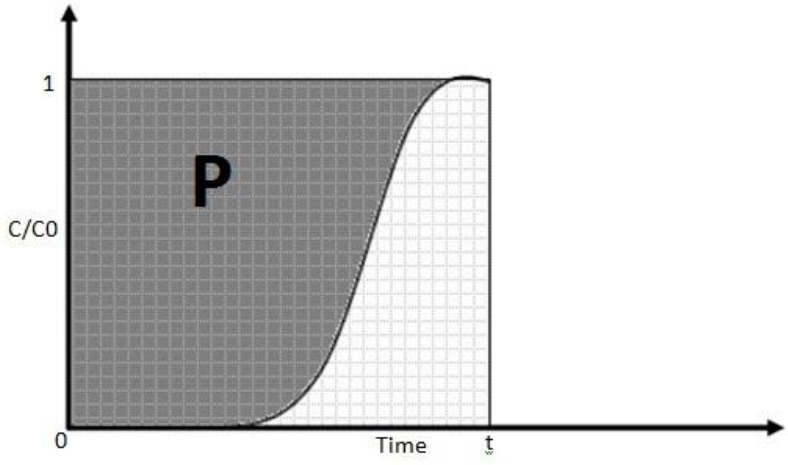

Figure 4-10 A typical breakthrough curve

To find the surface area above the breakthrough curve, the break point is defined as C/C_0=1 and the end of the breakthrough curve is where C/C_0 = 0.9.

Table 4-2- Comparison of CO_2 Conversion: TGA *vs*. Mass Balance (STP conditions)

	Conversion (Mass Balance)	Conversion (TGA-average)	Difference %
Pelletized Limestone 250-425 µm 0.5 L/min	0.93	0.87	6.89
Pelletized Limestone 250-425 µm 1 L/min	0.80	0.87	8.05
Pelletized Limestone 425-600 µm 0.5 L/min	0.85	0.88	3.41
Pelletized Limestone 425-600 µm 1 L/min	0.83	0.84	1.19

4-3-2-Natural Limestone

Figure 4-11 shows the effect of changing particle size and gas flow rate on the breakthrough time and breakthrough curve for natural limestone sorbent. Like pelletized limestone, it can be seen that smaller particles have a better performance (steeper breakthrough slope) due to their higher pore surface area. Hence, their overall CO_2 capture in comparison with larger particles is better.

Here, again, results show similar slopes for the breakthrough curves. Hence, changing the flowrate does not have much effect on the external mass transfer from bulk to the surface of the natural limestone.

Again, to confirm recorded data from the breakthrough curves and TGA, a mass balance in the gas phase based on Equation 4-2 was used and results from both methods were compared in Table 4-3. These results also confirm that the conversion which was calculated by a mass balance on the gas phase is almost equal to the average conversion which is obtained from the TGA.

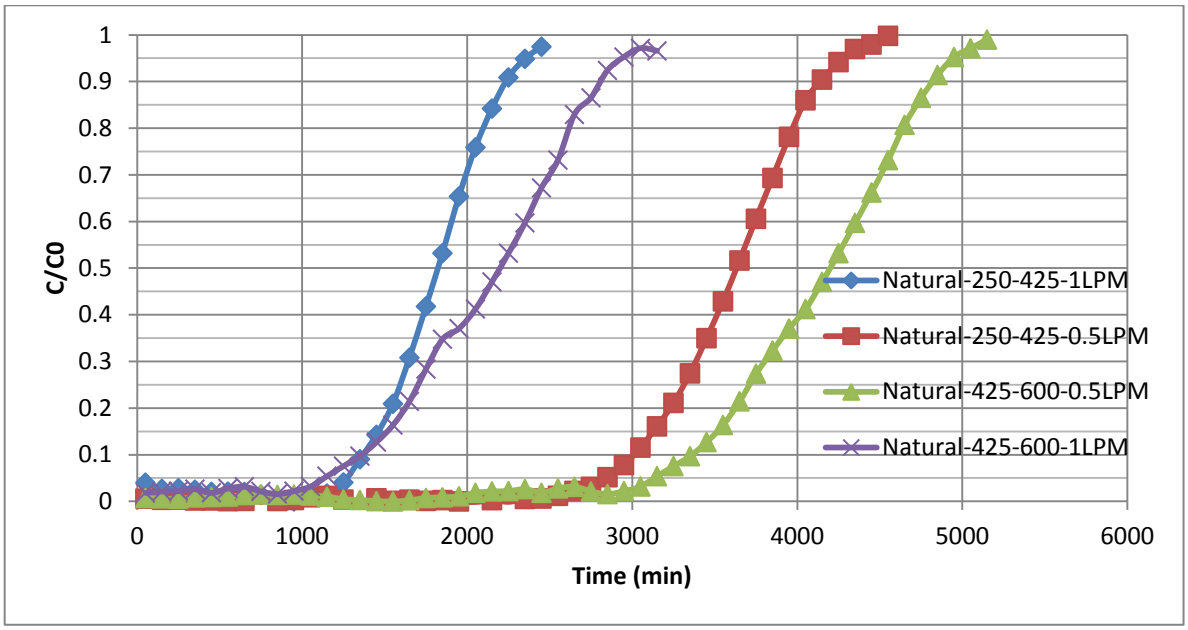

Figure 4-11 Effect of Particle size and gas flowrate on the breakthrough curve (Natural Limestone)

Moreover, Figure 4-12 show a uniform carbonation conversion along the bed in a selected run for natural limestone particles.

Table 4-3 Comparison of CO_2 Conversion: TGA *vs*. Mass Balance (STP conditions)

	Conversion (Mass Balance)	**Conversion (TGA-average)**	**Difference %**
Natural Cadomine 250-425 µm 0.5 L/min	0.89	0.91	2.19
Natural Cadomine 250-425 µm 1 L/min	0.80	0.89	10.11
Natural Cadomine 425-600 µm 0.5 L/min	0.86	0.92	6.52
Natural Cadomine 425-600 µm 1 L/min	0.89	0.95	6.31

Although in all cases (either natural or pelletize limestone), the mass loading of the sorbents in the reactor was the same, the breakthrough time of the pelletized limestone was shorter. The reason of this phenomenon is the formation of mayenite which is an inert compound.

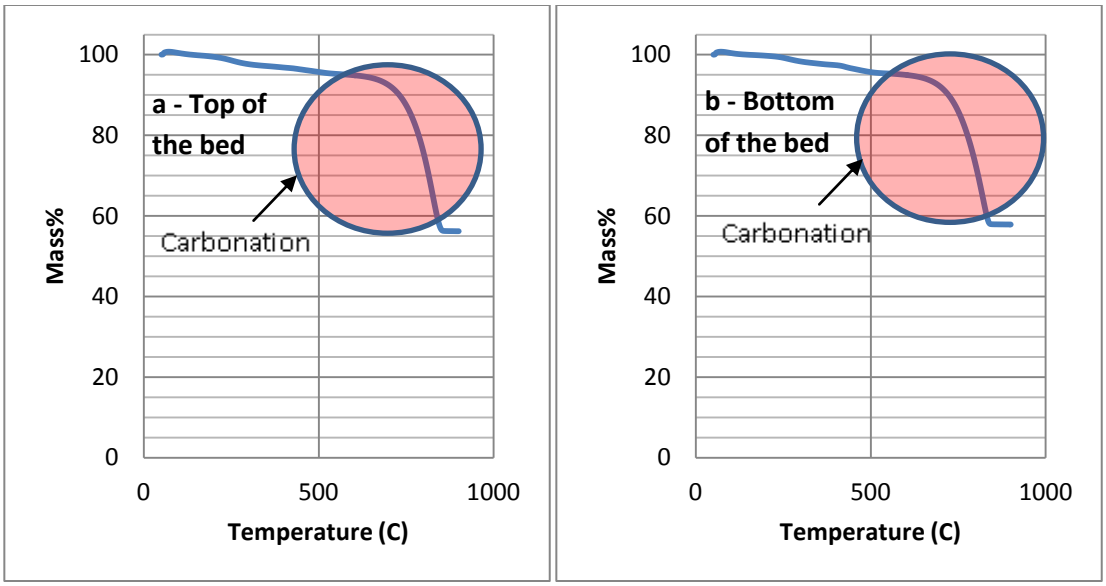

Figure 4-12 Hydration and Carbonation conversion of Pre hydrated Natural Limestone - (a-Top of the bed)- (b-Bottom of the bed) - humidified system (RH~55%) - 425-600 µm-0.53 LPM (1 barg, 20 °C)

4-4 Effect of Particle Type

Figures 4-13 and 4-14 show a comparison between breakthrough curves of pellets and natural limestone. While flowrate and particle size for both sorbents were the same, pellets have a higher surface area (Table 4-4). This leads to a sharper breakthrough curve, which shows that their capture is better than natural limestone sorbents.

Table 4-4 Pore surface area of sorbents

	Pelletized Limestone (250-425 µm)	**Pelletized Limestone (425-600 µm)**	**Natural Limestone (250-425 µm)**	**Natural Limestone (425-600 µm)**
Surface Area (m^2/g)	14.61	12.01	13.60	11.54

However, despite similar mass loading, breakthrough time of natural limestone particles is longer. This is due to the purity of natural limestone sorbents. In other words, pelletized limestone sorbents were made of 81% CaO and 10% binder while, natural limestone sorbents have almost 90% calcium oxide.

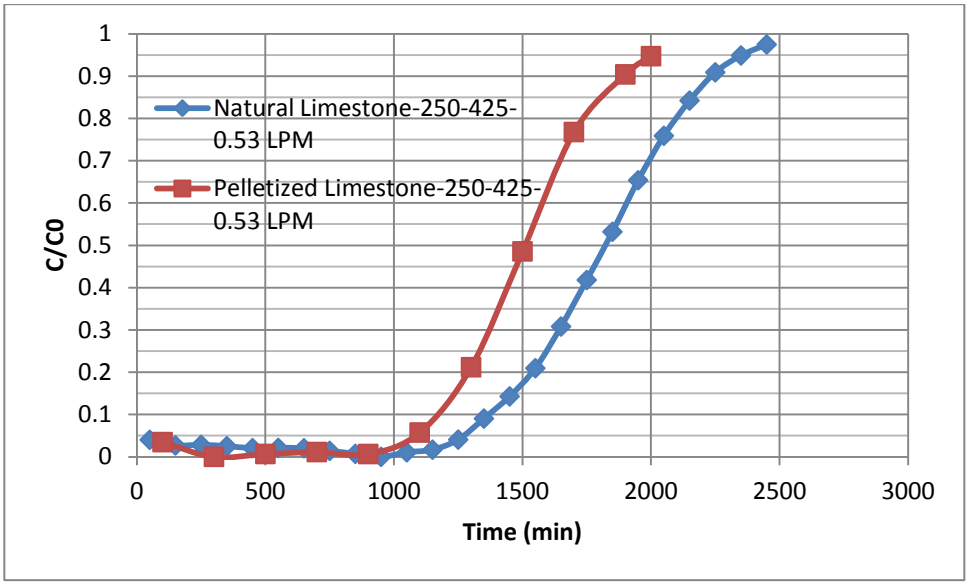

Figure 4-13 Effect of particle type on the breakthrough curves, Pelletized limestone *vs.* Natural limestone, 250-425 µm, 0.53 LPM (1barg, 20 °C)

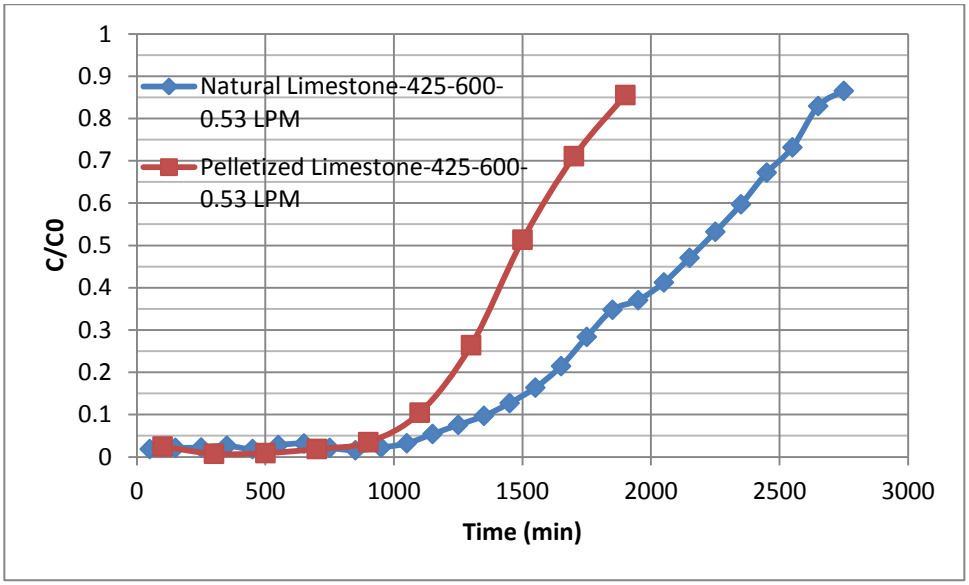

Figure 4-14 Effect of particle type on the breakthrough curves, Pelletized limestone *vs.* Natural limestone, 425-600 µm, 0.53 LPM (1barg, 20 °C)

4-5 Effect of relative humidity

The effect of relative humidity on the carbonation conversion was studied in section 4-2. Figure 4-15 also shows breakthrough curves of pelletized limestone with a range of particle size 425-600 µm. When the relative humidity is 78%, the slope of the curve is steepr. It can be concluded that the overall kinetics of the carbonation reaction for pelletized limestone at 78% relative humidity is greater than at 50% relative humidity. This phenomenon also confirms previous observation from literatures [26, 28 and 31].

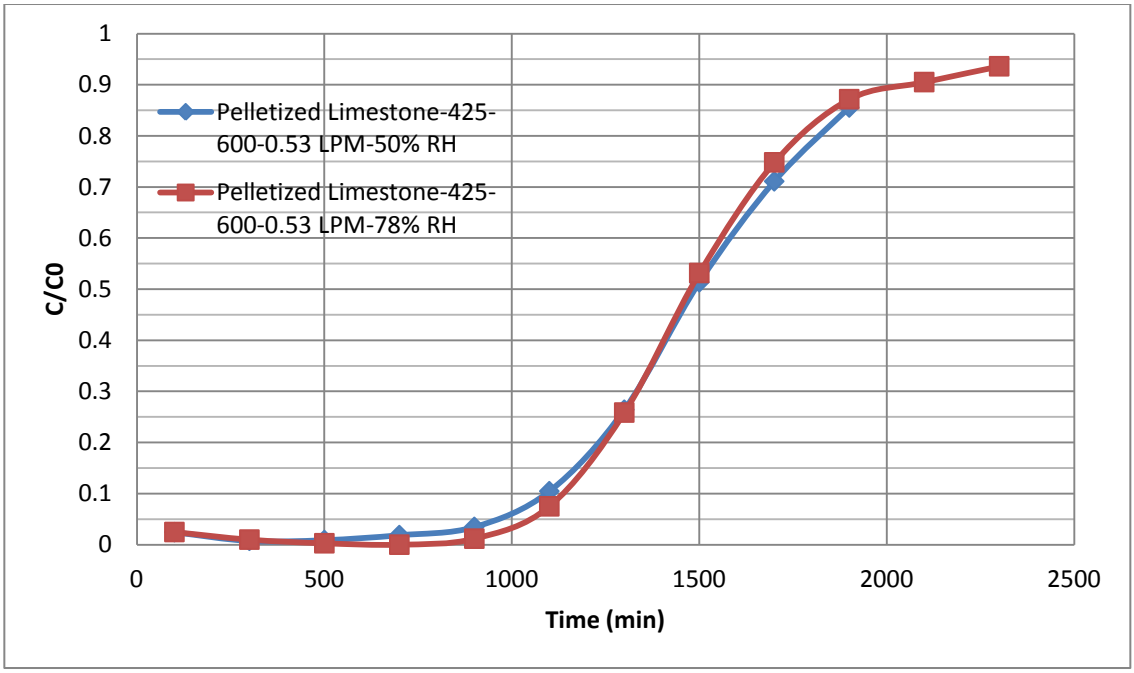

Figure 4-15 Effect of relative humidity on Pelletized limestone at similar condition (particle size, flowrate and temperature)

When relative humidity exceeds 40%, nano-droplets of water enhance further carbonation of the sorbents (section 2-4). While to minimum relative humidity which is needed for significant carbonation at ambient condition is 40%, the maximum relative

humidity is ~90%. At higher relative humidity, water droplets block pores of the sorbents and prevent CO_2 to react with $Ca(OH)_2$ [26].

4-6 Performance of sorbents in series of carbonation/calcination cycles

Figures 4-17 and 4-18 show the effects of a series of cycles on pelletized natural limestone. Sorbents were calcined for approximately 75 minutes and after each calcination, their surface area was measured by a BET (Figure 4-16). Carbonation of pellets was decreased from 80% to 71% after 9 cycles (10 cacinations). This is due to the sintering of sorbents while they are calcined at high temperature. Table 4-5 shows the carbonation conversion and surface area after selected cycles for pelletized limestone.

Table 4-5 Decay of carbonation reaction and surface area for pelletized limestone

	Carbonation Conversion (%)	Pore Surface Area (m^2/g)
1^{st}	80	12.01
2^{nd}	75	10.00
4^{th}	74	9.10
7^{th}	71	8.30
9^{th}	71	7.92

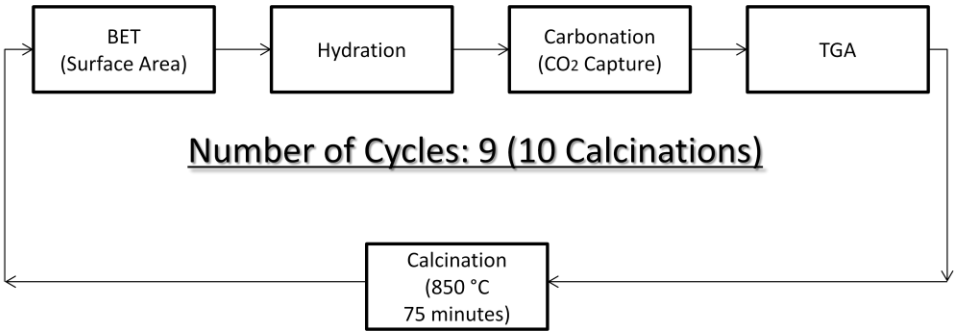

Figure 4-16 Schematic of CO_2 capture in series of cycles

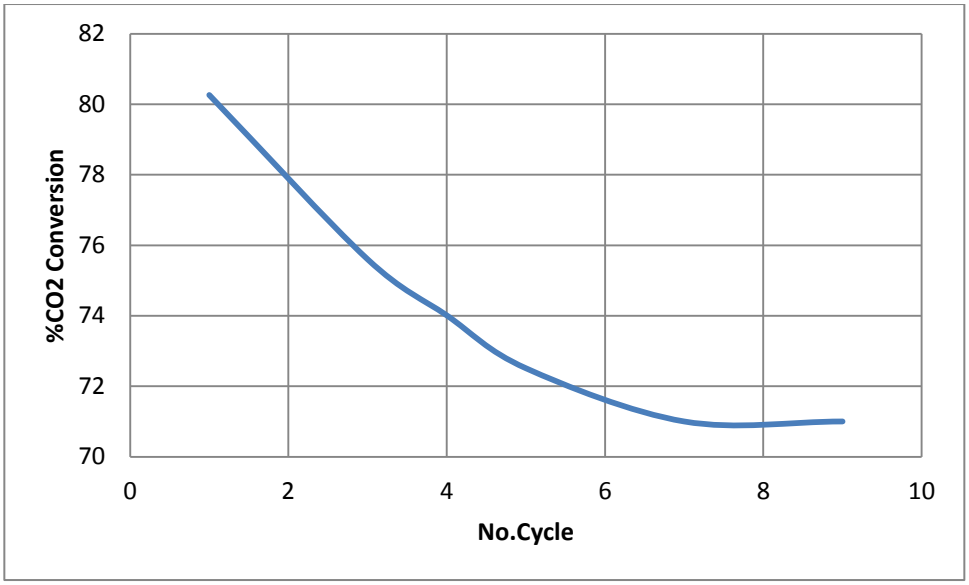

Figure 4-17 Carbonation conversion of Pelltized Limestone-425-600 µm- in series of cycle

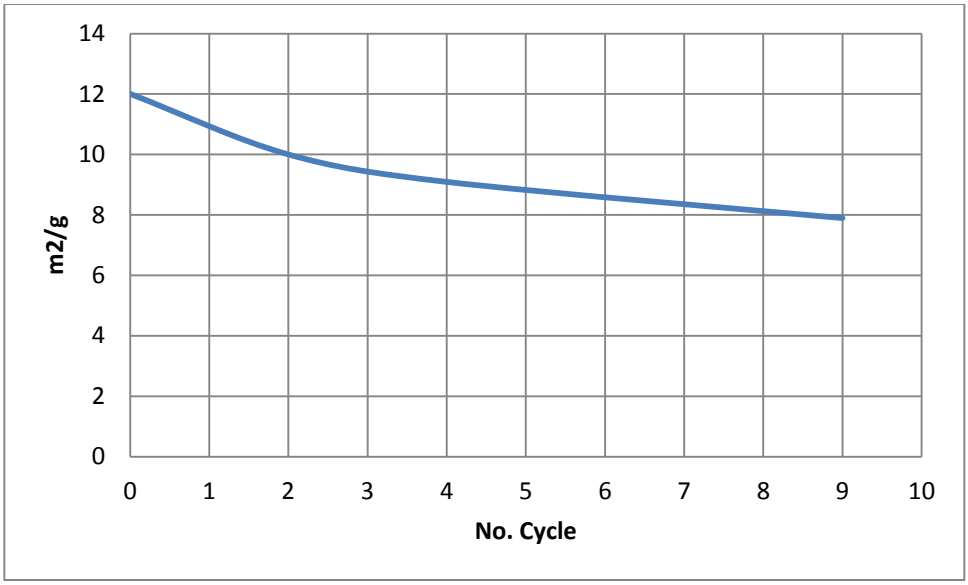

Figure 4-18 Surface area of pellets in series of cycle

Figures 4-19 and 4-20 show the performance of natural limestone sorbents in a series of carbonation/calcinations cycles (10 calcinations and 9 carbonations). Although the initial carbonation capacity of natural limestone sorbent is greater than pelletized limestone sorbents, after the same number of cycles, their decay due to the sintering is greater. Table 4-6 shows the trend of decay in carbonation conversion and pore surface area for natural limestone.

Table 4-6 Decay of carbonation reaction and surface area for natural limestone

	Carbonation Conversion (%)	Pore Surface Area (m^2/g)
1^{st}	93	11.54
2^{nd}	88	9.53
4^{th}	81	7.69
7^{th}	78	6.83
9^{th}	76	5.93

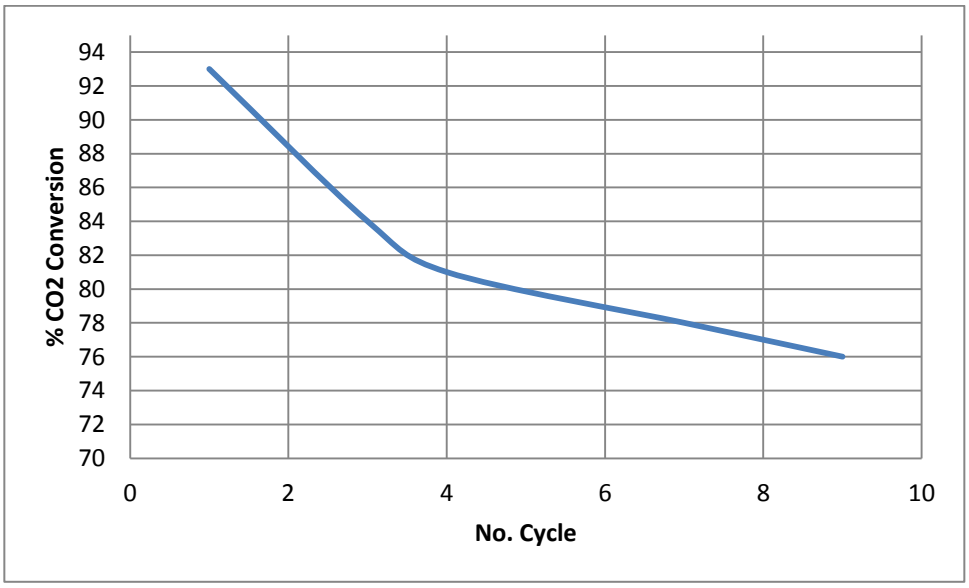

Figure 4-19 Carbonation conversion of Natural Limestone-425-600 µm in series of cycle

Table 4-7 compares performance of pelletized limestone and natural limestone sorbents before and after cycles. The excellent performance of the sorbents is due to the mild calcination condition (850 °C). Therefore, performance of the pelletized limestone at 920 °C and under CO_2 flow was studied as well. For this reason, sorbents are calcined at 920 °C for approximately 12 minutes and the results after 5 calcinations (4 cycles) are compared with previous conditions (calcinations at 850 °C and air for 75 minutes) in Table 4-8.

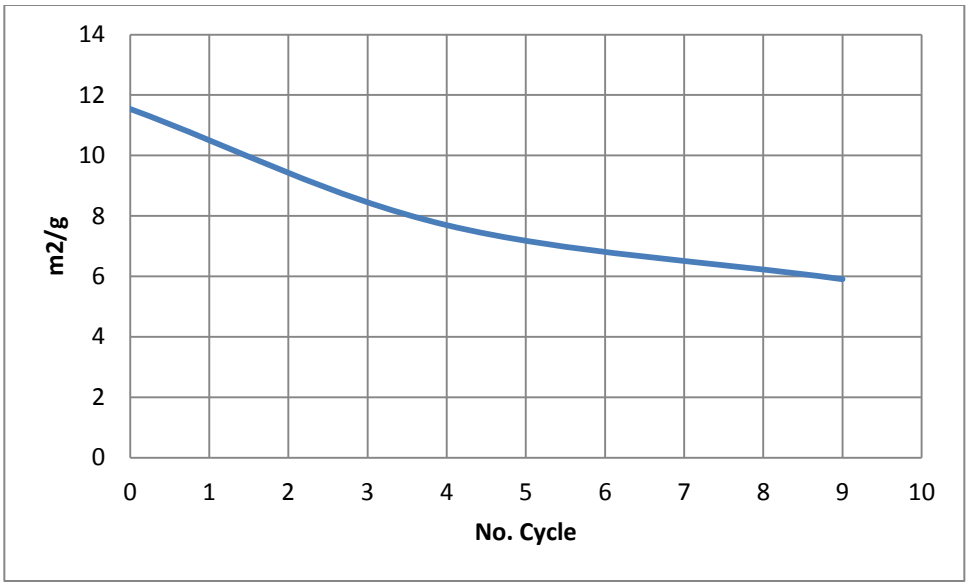

Figure 4-20 Surface area of natural limestone in series of cycle

Table 4-7 Performance of sorbents before and after 9 cycles: pelletized vs. natural limestone

	Initial Pore surface area	Pore surface area after 10 calcinations (m^2/g)	Carbonation conversion (Cycle#1)	Carbonation conversion (Cycle#9)
Pelletized Limestone (425-600 µm)	12.01	7.92	80%	71%
Natural Limestone (425-600 µm)	11.54	5.93	93%	76%

Table 4-8 Performance of pelletized limestone after 4 cycles of carbonation and calcination

Pelletized Limestone (425-600 µm)	Initial Pore surface area	Pore surface area after 5 calcinations (m^2/g)	Carbonation conversion (Cycle#1)	Carbonation conversion (Cycle#5)
Caclination with pure CO_2 at 920 °C	12.01	3.20	81%	59%
Calcination with air at 850 °C		9.10	80%	74%

High temperature results in sintering and drastic drop in pore surface area at the conditions of calcinations. Moreover, the carbonation conversion dropped to almost 60% after 4 cycles.

4-7- Fitting data with non-catalytic gas-solid reaction

In chapter 3, a non-catalytic gas-solid reaction model (shrinking core model) was presented. Unlike previous investigations on direct air capture via lime-based sorbents [26, 27, 29 and 31], this research uses larger-sized particles (250-425 μm and 425-600 μm). Hence, efforts to fit the breakthrough curves with the previously used surface reaction rate-limiting models will be unsuccessful since diffusional resistance becomes rate-limiting as the sorbents react with CO_2 producing a protective layer.

Data from experiments also confirm this hypothesis. At first, there is no protective layer ($CaCO_3$), hence the process is reaction controlled, while after formation of $CaCO_3$ diffusion dominates the CO_2 capture process. In order to fit data from breakthrough curves, the shrinking core model was adopted. In sections 4-3-1 and 4-3-2 it was explained that changing the gas flowrate did not change the shape of the breakthrough curves, therefore, it can be assumed that external mass transfer from bulk to the surface is negligible.

To find the relationship between $C_{CO2,in}$ and X at any point of the breakthrough curve a mass balance on a differential cross-section of the bed (Figure 4-21) based on the method proposed by Fenouil et al. [45] was used:

$$\frac{1}{4}\,\pi\,D^2 dZ \varepsilon_{fb}\,\frac{\partial C_{CO2,in}}{\partial t} = \qquad \text{Equation 4-3}$$

$$\frac{1}{4}\,\pi\,D^2 u_g C_{CO2}\left|Z - \frac{1}{4}\,\pi\,D^2 u_g C_{CO2}\right| Z + dZ - \frac{1}{4}\pi\,D^2 dZ(1-\varepsilon_{fb})C_{Ca(OH)2}\frac{\partial X}{\partial t}$$

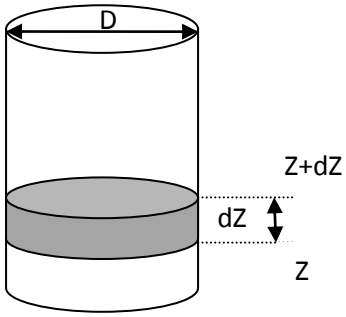

Figure 4-21 Differential cross sectional of the bed

$$\varepsilon_{fb}\frac{\partial C_{CO2,in}}{\partial t} = -u_g\frac{\partial C_{CO2,in}}{\partial Z} - (1-\varepsilon_{fb})C_{Ca(OH)2}\frac{\partial X}{\partial t} \qquad \text{Equation 4-4}$$

Transforming the following variables result in equation 4-11:

$\tau = t - Z/u_t$ Equation 4-5

$Z = (t-\tau)u_t$ Equation 4-6

While u_t is the moving velocity of the transition zone and calculated by an overall CO_2 mass balance over the bed:

$$\begin{bmatrix} Rate\ of\ flow\ of \\ CO_2 to\ the \\ fixed\ bed \end{bmatrix} - \begin{bmatrix} Rate\ of\ flow\ of \\ CO_2 out\ of\ the \\ fixed\ bed \end{bmatrix} = \begin{bmatrix} Rate\ of\ consumption \\ of\ adsorbent\ in \\ the\ fixed\ bed \end{bmatrix}$$

$$u_t = \frac{u_g C_{CO2,in}}{(1-\varepsilon_{fb})C_{Ca(OH)2}} \qquad \text{Equation 4-7}$$

Hence:

$$\frac{\partial C_{CO2,in}}{\partial t} = \frac{dC_{CO2,in}}{d\tau} \quad \text{Equation 4-8}$$

$$\frac{\partial X}{\partial t} = \frac{dX}{d\tau} \quad \text{Equation 4-9}$$

$$\frac{\partial C_{CO2,in}}{\partial Z} = -\frac{1}{u_t}\frac{dC_{CO2,in}}{d\tau} \quad \text{Equation 4-10}$$

$$\varepsilon_{fb}\left(1-\frac{u_g}{\varepsilon_{fb}u_t}\right)\frac{dC_{CO2,in}}{d\tau} + C_{Ca(OH)2}(1-\varepsilon_{fb})\frac{dX}{d\tau} = 0 \quad \text{Equation 4-11}$$

Boundary conditions at the end of the breakthrough, where the sorbents are completely converted are (it is assumed that at the end of the breakthrough, X reaches 1):

$C_{CO2}=C_{CO2,in}$ and X=1 at $\tau=0$

Integration of equation 4-11 results in equation 4-12:

$$\varepsilon_{fb}\left(1-\frac{u_g}{\varepsilon_{fb}u_t}\right)\left(C_{CO2}-C_{CO2,in}\right) + C_{Ca(OH)2}(1-\varepsilon_{fb})(X-1) = 0 \quad \text{Equation 4-12}$$

Substituting equation 4-7 into equation 4-12 gives the relationship between $C_{CO2,in}$ and X at any point of the breakthrough curve:

$$\frac{C_{CO2}}{C_{CO2,in}} = \frac{X-\frac{u_t\varepsilon_{fb}}{u_g}}{1-\frac{u_t\varepsilon_{fb}}{u_g}} \quad \text{Equation 4-13}$$

Figure 4-22 shows the relationship between X and t after the break point for pelletized limestone with a range of particle size between 250 and 425 μm and 0.5 L/min (STP conditions) volumetric flowrate.

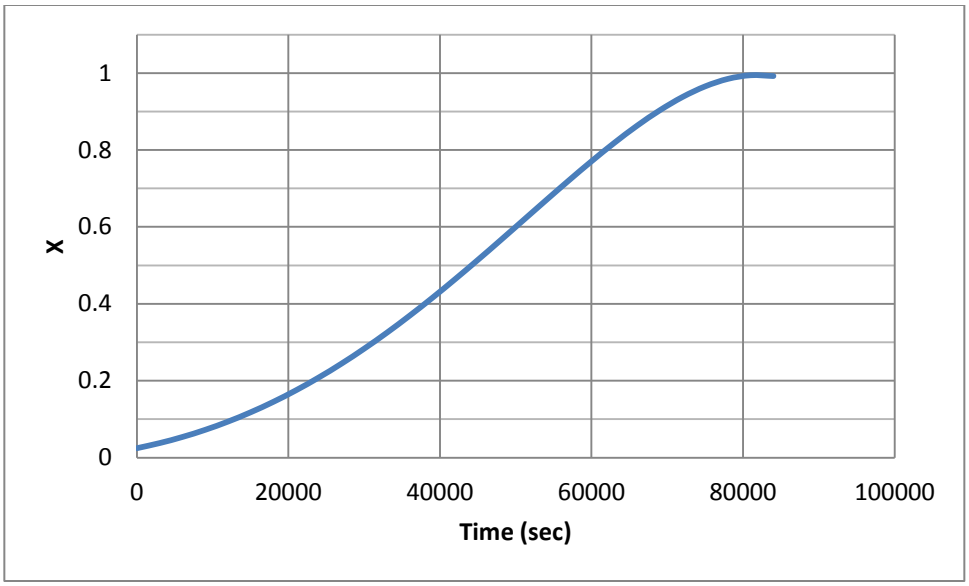

Figure 4-22 Conversion of Pelletized Limestone using Equation 4-13

To identify the time at which the rate controlling mechanism changes from surface reaction to diffusion, a first derivative function ($\frac{\Delta X}{\Delta t}$) is used. Figure 4-23 shows results of this method for the same data of Figure 4-22:

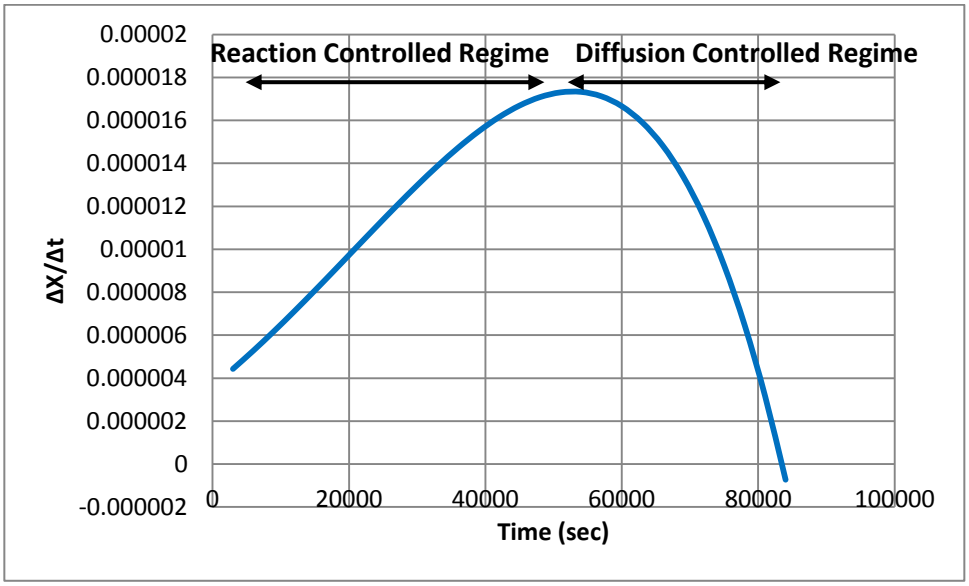

Figure 4-23 dx/dt as a function of time (based on Figure 4-22)

To find the surface reaction constant (K_s), data from the first regime are fit with equation 2-9 whereas data from the second regime are fit with equation 2-8 to estimate the effective diffusivity constant (D_e) . Slopes of these curves represent $\tau_{R,SC}$ (Figure 4-24) and τ_{DP}(Figure 4-25).

$$K_S = \frac{\rho_s R}{b\tau_{R,SC} C_{CO2,in}}$$ Equation 4-14

$$D_e = \frac{\rho_s R^2}{6b\tau_{DP} C_{CO2,in}}$$ Equation 4-15

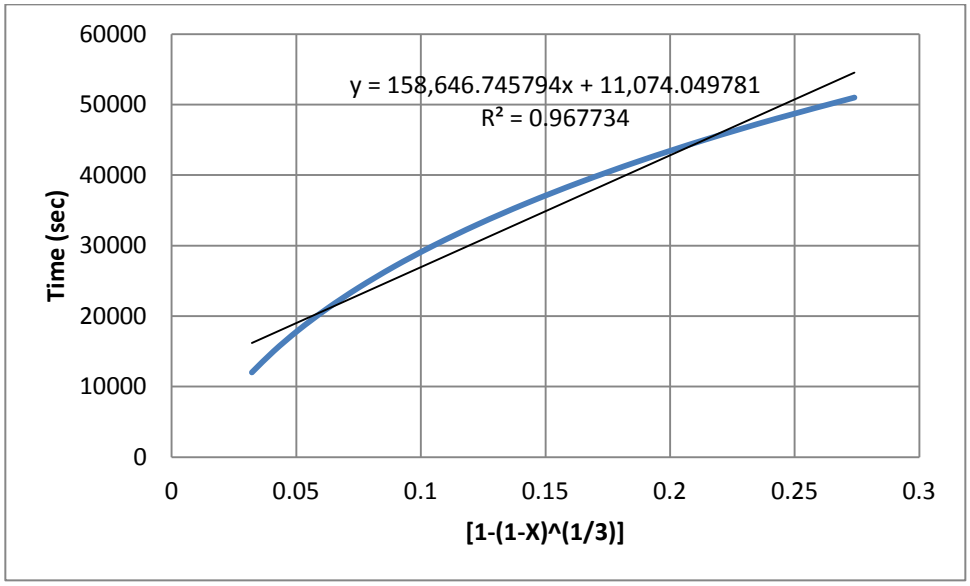

Figure 4-24 Slope extraction for reaction controlled regime

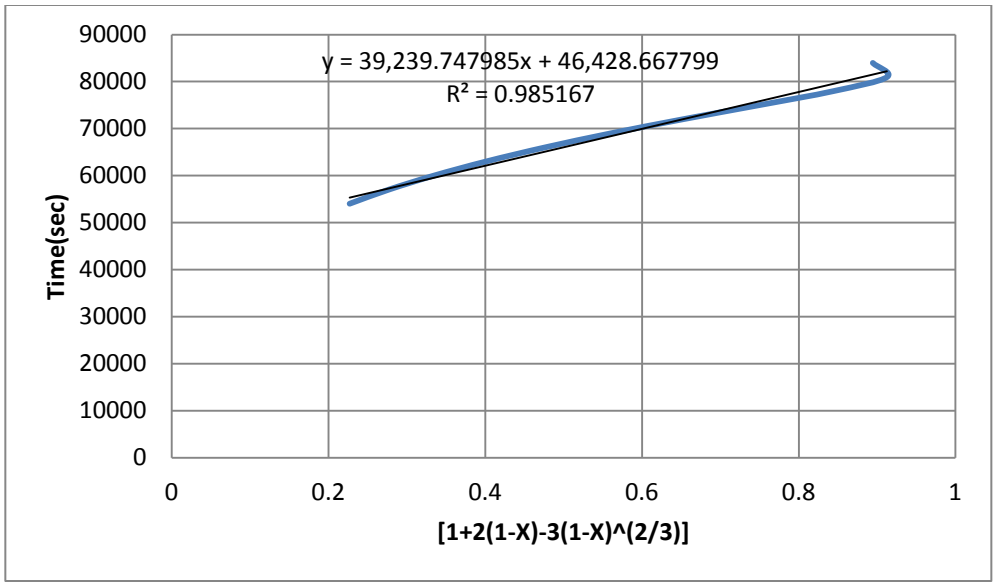

Figure 4-25 Slope extraction for diffusion controlled regime

Results from fitting different data series of pelletized natural limestone with the aforementioned procedure were summarized in Table 4-9. Smaller particles have greater surface area (Table 3-2) and this improves their effective diffusion constant.

Table 4-9 Reaction constant and effective diffusivity constant of pelletized limestone (STP conditions)

	250-425 µm 0.5 L/min	250-425 µm 1 L/min	425-600 µm 0.5 L/min	425-600 µm 1 L/min
Diffusion Controlled D_e(m^2/s)	5.164×10^{-8}	4.029×10^{-8}	3.118×10^{-8}	2.722×10^{-8}
Reaction Controlled K_s(m/s)	4.541×10^{-4}	6.266×10^{-4}	5.253×10^{-4}	4.678×10^{-4}

As seen in 4-3-1 the effect of flow rate is negligible on the shape of the breakthrough curve. Hence, mass transfer coefficient, K_g, from bulk to the surface of the particle was assumed to be negligible. Results in Table 4-9 also confirm this hypothesis. While the flowrate increases from 0.5 L/min to 1 L/min, effective diffusivity, D_e, and surface reaction constant, K_s, for particles with the same size range remain almost constant. The average effective diffusivity is 4.6×10^{-8} and 2.9×10^{-8} m^2/s for particle size of 250-425 µm and 425-600 µm respectively. However, the surface reaction constant is almost similar for this type of sorbent and its average is 5.2×10^{-4} m/s.

In order to quantify and compare kinetics of pelletized and natural limestone sorbents, the same approach is used for natural limestone particles.

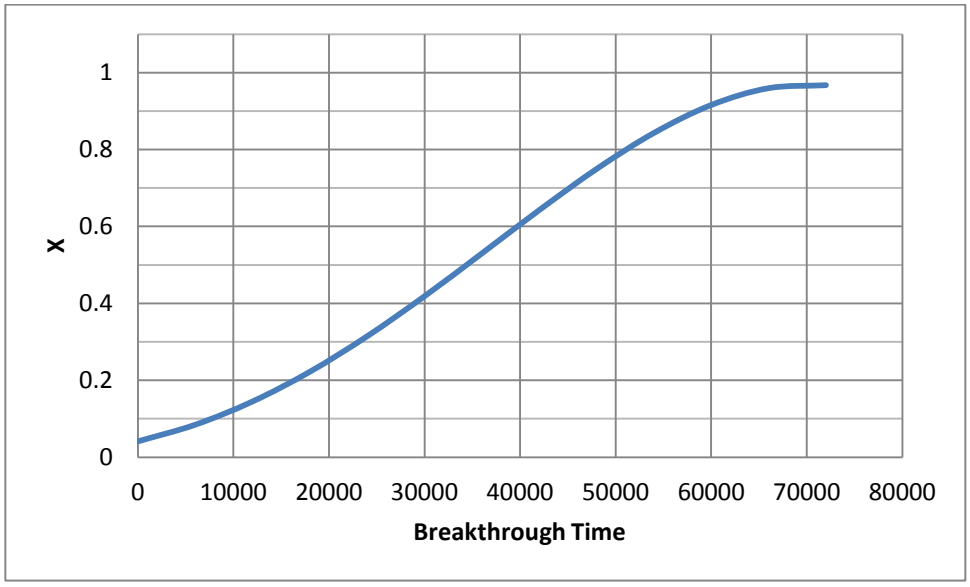

Figure 4-26 Conversion of Natural Limestone using Equation 4-13

Figure 4-27 shows how the regime changes from chemical reaction controlled to diffusion controlled. Figures 4-28 and 4-29 show how data from the breakthrough curve

(capture by natural limestone: 250-425 µm - 1 LPM at STP conditions) fit with those regimes:

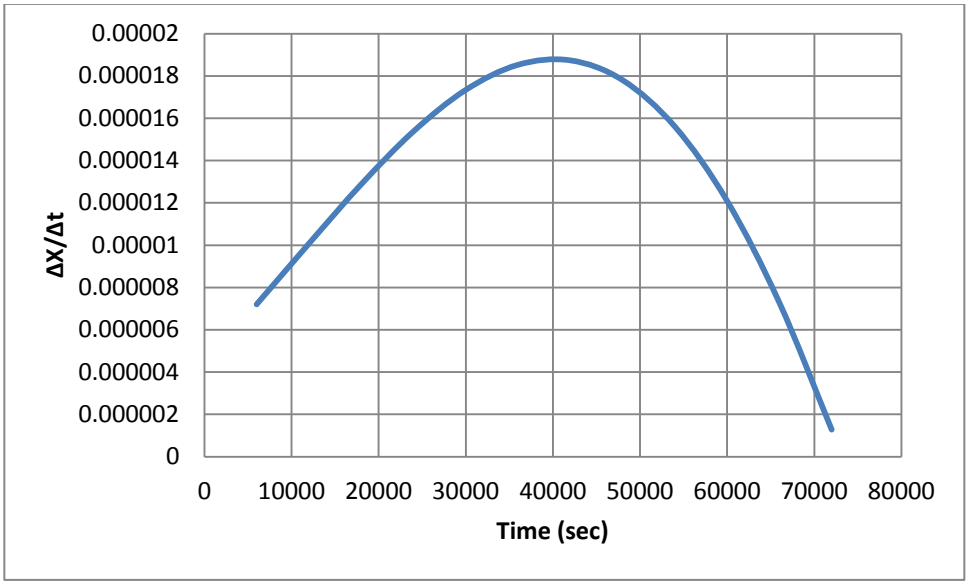

Figure 4-27 dx/dt as a function of time (based on Figure 4-26)

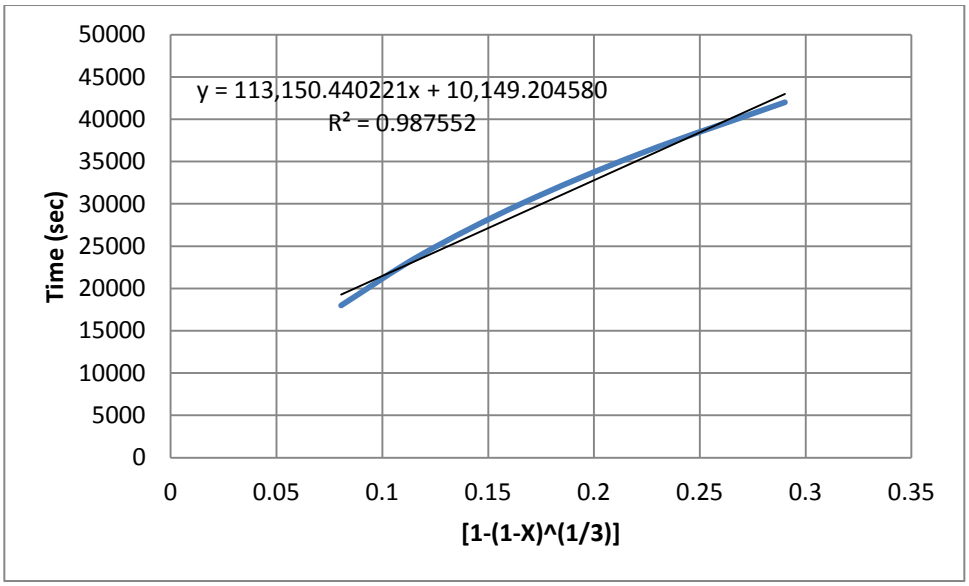

Figure 4-28 Slope extraction for reaction controlled regime

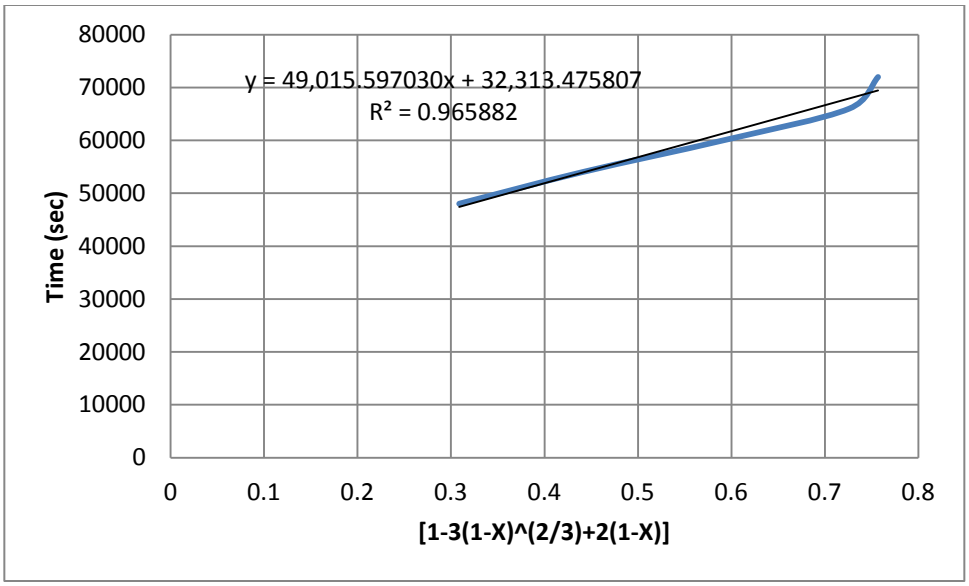

Figure 4-29 Slope extraction for reaction controlled regime

K_S and D_e are calculated from the slope of the curves, based on Equations 4-14 and 4-15. Table 4-10 summarizes the surface reaction rate constant and effective diffusivity for each run. Again, results confirm the effect of the K_g on overall kinetics of the reaction is negligible. Furthermore, K_S for all cases is similar and its value is also close to the surface reaction rate constants which were obtained from pelletized limestone.

Effective diffusivity, D_e, for smaller particles is greater than larger particles. Comparing these values (K_S and D_e) for both sorbents shows us that the overall kinetics of the sorbents is different due to D_e which is attributed to the surface area.

However, effective diffusivity of pelletized limestone is greater than natural limestone. As instance, average D_e is 2.9×10^{-8} m^2/s for pelletized limestone with particle range of 425-600 µm, while its average value is 7.9×10^{-9} m^2/s for natural limestone with

the same particle size. This arises from the binder that increases the pore surface area of the sorbent.

Table 4-10 Reaction constant and effective diffusivity constant of natural limestone (STP conditions)

	250-425 µm 0.5 L/min	250-425 µm 1 L/min	425-600 µm 0.5 L/min	425-600 µm 1 L/min
Diffusion Controlled D_e(m^2/s)	2.4061×10^{-8}	2.158×10^{-8}	7.489×10^{-9}	8.336×10^{-9}
Reaction Controlled K_s(m/s)	5.395×10^{-4}	6.177×10^{-4}	3.724×10^{-4}	5.866×10^{-4}

Since in this research CaO-based sorbents first react with water and become hydrated as Equation 3-1, and then are exposed to humidified air which enhances the overall reaction rate of the sorbents, results show a greater surface reaction rate constant and effective diffusion constant compared with to the other approaches at higher temperature and dry system with CaO based sorbents [35].

Finally, the effect of relative humidity on the overall reaction rate is quantified. As it was reported in other studies [31 and 33], the effect of relative humidity is observed in the diffusion-controlled region, where water diffuses in the pores of the sorbent and enhances the CO_2 diffusion to the bulk of the particle. Results from Table 4-11 confirm the previous explanation about the effect of relative humidity.

Table 4-11 Reaction constant and effective diffusivity constant of pelletized limestone: 50% RH *vs.* 78% RH

	425-600 µm 1 L/min (RH~50%)	425-600 µm 1 L/min (RH~78%)
Diffusion Controlled D_e(m^2/s)	2.72×10^{-8}	7.16×10^{-8}
Reaction Controlled K_s(m/s)	4.67×10^{-4}	9.58×10^{-4}

Chapter 5

Conclusions and Recommendations

5-1- Conclusions

The performance of the natural limestone from Cadomin and the pelletized limestone which is 90% natural limestone and 10% calcium aluminum cement (CA-14) were compared as sorbent for CO_2 capture from air at ambient conditions in a fixed bed reactor. Observations show that pre-hydration of the sorbents leads to a uniform carbonated bed. Moreover, relative humidity is an important parameter on the carbonation of sorbents. In a dry system (RH~0%) the breakthrough time was very short and the carbonation conversion of the sorbents was low in comparison with a system with 55% relative humidity.

Comparing the performance of two sorbents in 9 series of carbonation and calcination cycles at 850 °C under air show that due to the presence of the binder in pelletized limestone, their decay in carbonation conversion (from 80% to 71%) was less than natural limestone (from 93% to 76%). Moreover, the trend of decay in pores surface area (from 12.01 m^2/g to 7.92 m^2/g) comparing to natural limestone (from 11.54 m^2/g to 5.93 m^2/g) shows that pelletized limestone does not sinter as much as natural limestone. Hence, pelletized limestone sorbents were chosen to be studied further at oxy-fuel conditions (920 °C under pure CO_2). However, their carbonation conversion (from 81% to 59%) and pore surface area (from 12.01 to 3.20 m^2/g) dropped drastically after 4 cycles.

The shrinking core model was used for mathematical modeling of data from breakthrough curves. Based on preliminary observations from breakthrough curves, changing the flowrate does not have effect on the overall kinetics of the reaction. Hence, the mass transfer resistance from bulk to the surface was assumed negligible. The carbonation of sorbents can be divided in 2 regions: reaction controlled and diffusion controlled. Initially, the carbonation rate is dominated by the chemical reaction kinetics on the surface of the particle. As the reaction proceeds, formation of the product layer on the surface of the particles, leads the reaction to the diffusion controlled zone. Results from mathematical modeling also confirm aforementioned hypothesizes. The change of the flowrate does not affect the effective diffusivity or the surface reaction constant of sorbents. Moreover, the surface reaction constant of smaller particles is similar to larger particles, while their effective diffusivity was greater due to their higher pore surface area. The average value of the effective diffusivity, as it was expected, was greater for pelletized limestone comparing to natural limestone. This would be attributed to their higher pore surface area. Therefore, the main difference of the pelletized limestone and natural limestone in CO_2 capture at ambient conditions arises from the higher effective diffusivity of pelletized limestone.

5-2- Recommendations

Based on data analysis, results and objectives of this thesis, the following recommendations would result in the improvement of the air capture process:

- Unlike fluidized bed reactors, in fixed bed reactors particles do not have collision during the capture. Hence, 10% calcium aluminum cement as binder could be decreased to 5%.
- Series of capture and regeneration experiments were conducted at oxy-fuel conditions (920 °C under pure CO_2). Decay in carbonation conversion and pore surface area could be decreased if the calcinations time is shorter (e.g., less than 12 minutes).
- Shrinking core model is a simple gas-solid reaction model. Other models, such as grain model and random pore model would better detail the kinetics of the reaction. However, using these models needs more parameters that require specialized equipment for measurement (e.g., mass measurement during the experiment).
- In order to compare the feasibility of direct air capture with lime-based sorbents to the other systems, further studies on this method is needed.
- Since these sorbents show acceptable performance for CO_2 capture from air at ambient conditions, their performance would be studied for other CO_2 dilute sources such as natural gas.

References:

1 - *Climate Change 2007 – The Physical Science Basis.* 2007, International Panel on Climate Change.

2 - Lüthi, D., M.L. Floch, B. Bereiter, T. Blunier, J.M. Barnola, U. Siegenthaler, D. Raynaud, J. Jouzel, H. Fischer, K. Kawamura and T.F. Stocker. 2008. *High-resolution carbon dioxide concentration record 650,000-800,000 years before present*, Nature 453: 379-382.

3 - Petit J.R., Jouzel J., Raynaud D., Barkov N.I., Barnola J.M., I. Basile, M. Bender, J. Chappellaz, M. Davis, G. Delaygue, M. Delmotte, V. M. Kotlyakov, M. Legrand, V.Y. Lipenkov, C. Lorius, L. PÉpin, C. Ritz, E. Saltzman and M. Stievenard. 1999, *Climate and Atmospheric History of the Past 420,000 years from the Vostok Ice Core, Antarctica*, Nature 399: 429-436.

4 - Earth System Research Laboratory - *Mauna Loa observatory* [cited 2014; available from: http://www.esrl.noaa.gov/gmd/obop/mlo/]

5 - *CO_2 Emissions from Fuel Combustion.* 2011, International Energy Agency.

6 – *Carbon Capture and Storage.* 2005, International Panel on Climate Change.

7 - Blamey, J., Anthony, E.J., Wang, J., and Fennell, P.S., *The calcium looping cycle for large-scale CO_2 capture.* Progress in Energy and Combustion Science, 2010. 36(2): p. 260-279.

8 – *CO_2 Emissions from Fuel Combustion*, 2013. International Energy Agency.

9 - Ranjan, M. and Herzog, H.J., *Feasibility of air capture*, Energy Procedia, 2011. 4: p. 2869-2876.

10 - Lackner, K.S., Grimes, P., Ziock, H.J., *Capturing Carbon Dioxide from Air*. Proceedings of the first international sequestration conference, 2001. Session 78: capture, pp 1-15

11 - Moriatry, P. and Honnery, D., *A human needs approach to reducing atmospheric carbon.* Energy Policy, 2010. 38: p. 695-700.

12 - Mahmoudkhani, M. and Keith, D.W., *Low energy sodium hydroxide recovery for CO_2 capture from atmospheric air-Thermodynamic analysis.* International Journal of Greenhouse Gas Control, 2009. 3: p. 376-384.

13 - Keith, D.W., MinH Ha-Duong, Joshuah K.Stolaroff, *Climate Strategy With CO_2 Capture from The Air*, Climate Change (2005).

14 - V. Nikulshina, D. Hirsch, M. Mazzotti, A. Steinfield, *CO_2 capture from air and co-production of H2 via the $Ca(OH)_2$-$CaCO_3$ cycle using concentrated solar power-thermodynamic analysis*, Energy 31 (2006) 1379-1389.

15 - Carbon Engineering - *INDUSTRIAL-SCALE CAPTURE OF CO_2 FROM AMBIENT AIR* [cited 2014; available from: http://carbonengineering.com/air-capture].

16 - Mahmoudkhani M. ,Heidel K.R. ,Ferreira J.C. ,Keith D.W. , Cherry R.S. ,*Low energy packed tower and caustic recovery for direct capture of CO_2 from air*, Energy Procedia, (2009) 1535-1542

17 - Foley, J., and Ramankutty N. (2004). *A Primer on the Terrestrial Carbon Cycle: What We Don't Know But Should.* Chapter 14 in The Global Carbon Cycle. Eds. C.B. Field and M.R. Raupach, Island Press, Washington DC. pp. 526.

18 - Nakicenovic N. et al., (2000). *Emissions Scenarios. A Special Report of Working Group III of the IPCC.* Cambridge University Press. pp. 599.

19 - Jayant. S, W. Makundi, L. Dale, P. Chan, K. Andrasko, *GHG Mitigation Potential, Costs and Benefits in Global Forests: A Dynamic Partial Equilibrium Approach,* 2006, Energy Journal;Multi-Greenhouse Gas Mitigation, 27: p127

20 - Choi, S., J.H. Drese, P.M. Eisenberger, and C.W. Jones, *Application of Amine-Tethered Solid Sorbents for Direct CO_2 Capture from the Ambient Air*, 2011, Environmental Science & Technology, 45: 2420–2427.

21 - Sculley, J.P. and H.C. Zhou, *Enhancing Amine-Supported Materials for Ambient Air, 2012,* Capture Angewandte Chemie International Edition, 51: 12660–12661

22 – Manovic, V., E.J. Anthony, *CaO-Based Pellets Supported by Calcium Aluminate Cements for High-Temperature CO_2 Capture,* 2009, Environmental Science & Technology, 43: 7117–7122.

23 - Manovic, V., E.J. Anthony, *CO_2 Carrying Behavior of Calcium Aluminate Pellets under High Temperature/High-CO_2 Concentration Calcination Conditions,* 2010, Industrial & Engineering Chemistry Research, 49: 6916–6922

24 - Manovic, V., Y. Wu, I. He and Edward J. Anthony, *Spray Water Reactivation Pelletization of Spent CaO-based Sorbents from Calcium Looping Cycles,* 2012*,* Environmental Science and Technology, 46: 12720−12725.

25 - Manovic, V., E.J. Anthony, *Long-Term Behavior of CaO-Based Pellets Supported by Calcium Aluminate Cements in a Long Series of CO_2 Capture Cycles,* 2009, Industrial & Engineering Chemistry Research, 48: 8906-8912.

26 - Beruto, D.T., R. Botter, *Liquid like H_2O adsorption layers to catalyze the $Ca(OH)_2/CO_2$ solid-gas reaction and to form a non-protective solid product layer at 20 °C*, 2000, Journal of the European Ceramic Society, 20: 497-503

27 - Dheilly, R.M., J. Tudo, Y.Sebaibi, M. Queneudec, *Influence of storage conditions on the carbonation of powdered $Ca(OH)_2$*, 2002, Construction and Building Materials, 16: 155-161

28 - Kalinkin, A.M., E.V. Kalinkina, O.A. Zalkind, T.I. Makarova, *Chemical interaction of calcium oxide and calcium hydroxide with CO_2 during mechanical activation*, 2005, Inorganic Materials, 41: 1073-1079

29 - Pontiga, F., J.M. Valverde, H. Moreno, F.J. Duran-Olivencia, *Dry gas-solid carbonation in fluidized beds of $Ca(OH)_2$ and nanosilica/$Ca(OH)_2$ at ambient temperature and low CO_2 pressure*, 2013, Chemical Engineering Journal, 222: 546-552

30 - Yang, R.Y., R.P. Zou, A.B. Yu, *Effect of material properties on the packing of fine particles*, 2003, Journal of Applied Physics, 94: 3025-3034

31 - Nikulshina, V., M.E. Gavez, A. Steinfeld, *Kinetic anaylisys of the carbonation reactions for the capture of CO_2 from air via the $Ca(OH)_2$-$CaCO_3$-CaO solar thermochemical cycle,* 2007, Chemical Engineering Journal 129: 75-83

32 - Shih, S.M., C.S. Ho, Y.S. Song, J.P. Lin, *Kinetics of the reaction of $Ca(OH)_2$ with CO_2 at low temperature*, 1999, Industrial & Engineering Chemistry Research, 38: 1316-1322

33 - Donat, F., N. Florin, E.J. Anthony, P. Fennel, *The influence of high-temperature steam on the reactivity of CaO sorbents for CO_2 capture*, 2011, Environmental Science & Technology, 46: 1262–1269.

34 - Symonds, R.T., D.Y. Lu, R.W. Hughes, E.J. Anthony, A. Macchi, *CO_2 capture from simulated syngas via cyclic carbonation/calcinations for a naturally occurring limestone: Pilot-plant testing*, 2009, Industrial & Engineering Chemistry Research, *48* (18), pp 8431–8440

35 – Zhiming, Z., P. Xu, M. Xie, Z. Cheng, W. Yuan, *Modeling of the carbonation kinetics of a synthetic CaO-based sorbent*, 2013, Chemical Engineering Science, 95: 283-290

36 - Levenspiel, O., *Chemical Reaction Engineering*, 2nd Edition, chapter 13, 357-371

37 - Akehata, T., Sato K., *Flow distribution in packed beds,* 1958*,* Chemical Engineering Japan Journal, 22: 430-436

38 - Gunn, D.J., *Mixing in Packed and Fluidized Beds*. 1996, Chemical Engineering Journal, 153-172

39 - Gunn, D.J., C. Pryce, *Dispersion in packed beds*, 1969, Trans IChemE 47:T341-T350

40 - Stephenson, J.L., W.E. Stewart, *Optical measurement of porosity and fluid motion in packed beds*, 1986, Chemical Engineering Science 42:2161-2170

41 - Han, NW., J. Bhakta, RG. Carbonelli, *Longitudinal and lateral dispersion in packed beds: effect of column length and particle size distribution.* 1985, AIChE Journal 31:277-288

42 - Taylor, G., *Dispersion of soluble matter in solvent flowing slowly through a tube,* 1953, Proceedings of the Royal Society A, 219:186-203

43 - Ribeiro, A.M., P. Neto, C. Pinho, Mean Porosity and Pressure Drop Measurements in Packed Beds of Monosized Spheres: Side Wall Effects, 2010, International Review of Chemical Engineering, 2:40-46

44 - Ranade V.V., R. Chaudhari, P.R. Gunjal, *Trickle Bed Reactors: Reactor Engineering & Applications,* chapter 4

45 - Fenouil, L. A., S. Lynn, *Design of Entrained-Flow and Moving-, Packed,and Fuidized-Bed Sorption Systems: Grain-Model Kinetics for Hot Coal-Gas Sulphurization with Limestone,* 1996, Industrial and Engineering Chemistry Research, 35 (2), 1024-1043